

Implications for the Constrained MSSM from a new prediction for $b \rightarrow s\gamma$

This content has been downloaded from IOPscience. Please scroll down to see the full text.

JHEP07(2007)075

(<http://iopscience.iop.org/1126-6708/2007/07/075>)

View [the table of contents for this issue](#), or go to the [journal homepage](#) for more

Download details:

IP Address: 129.31.210.161

This content was downloaded on 23/08/2016 at 12:47

Please note that [terms and conditions apply](#).

You may also be interested in:

[Updated constraints from B physics on the MSSM and the NMSSM](#)

Florian Domingo and Ulrich Ellwanger

[The impact of priors and observables on parameter inferences in the constrained MSSM](#)

Roberto Trotta, Farhan Feroz, Mike Hobson et al.

[Charged Higgs bosons in minimal supersymmetry: updated constraints and experimental prospects](#)

David Eriksson, Farvah Mahmoudi and Oscar Stål

[Flavour violation in anomaly mediated supersymmetry breaking](#)

B.C. Allanach, G. Hiller, D.R.T. Jones et al.

[Light charged Higgs at the beginning of the LHC era](#)

Gabriela Barenboim, Paride Paradisi, Oscar Vives et al.

[Challenging SO\(10\) SUSY GUTs with family symmetries through FCNC processes](#)

Michaela E. Albrecht, Wolfgang Altmannshofer, Andrzej J. Buras et al.

Implications for the Constrained MSSM from a new prediction for $b \rightarrow s\gamma$

Leszek Roszkowski

*Department of Physics and Astronomy, University of Sheffield,
Sheffield S3 7RH, England, and
Theory Division, CERN, CH-1211 Geneva 23, Switzerland
E-mail: L.Roszkowski@sheffield.ac.uk*

Roberto Ruiz de Austri

*Departamento de Física Teórica C-XI and Instituto de Física Teórica C-XVI,
Universidad Autónoma de Madrid, Cantoblanco,
28049 Madrid, Spain
E-mail: rruiz@delta.ft.uam.es*

Roberto Trotta

*Astrophysics Department, Oxford University
Denys Wilkinson Building, Keble Road, Oxford OX1 3RH, United Kingdom
E-mail: rxt@astro.ox.ac.uk*

ABSTRACT: We re-examine the properties of the Constrained MSSM in light of updated constraints, paying particular attention to the impact of the recent substantial shift in the Standard Model prediction for $BR(\bar{B} \rightarrow X_s\gamma)$. With the help of a Markov Chain Monte Carlo scanning technique, we vary all relevant parameters simultaneously and derive Bayesian posterior probability maps. We find that the case of $\mu > 0$ remains favored, and that for $\mu < 0$ it is considerably more difficult to find a good global fit to current constraints. In both cases we find a strong preference for a focus point region. This leads to improved prospects for detecting neutralino dark matter in direct searches, while superpartner searches at the LHC become more problematic, especially when $\mu < 0$. In contrast, prospects for exploring the whole mass range of the lightest Higgs boson at the Tevatron and the LHC remain very good, which should, along with dark matter searches, allow one to gain access to the otherwise experimentally challenging focus point region. An alternative measure of the mean quality-of-fit which we also employ implies that present data are not yet constraining enough to draw more definite conclusions. We also comment on the dependence of our results on the choice of priors and on some other assumptions.

KEYWORDS: Supersymmetry Phenomenology, Supersymmetric Standard Model.

Contents

1. Introduction	1
2. The analysis	4
2.1 Theoretical framework	4
2.2 Constraints	5
3. Results	8
3.1 Implications for the CMSSM parameters	8
3.2 Implications for collider searches	17
3.3 Implications for direct detection of Dark Matter	20
3.4 Correlations among observables	24
4. Summary and conclusions	25

1. Introduction

Among various possible sets of boundary conditions that one can impose on the multi-dimensional parameter space of the effective, low-energy Minimal Supersymmetric Standard Model (MSSM), [1] the by far most popular choice is the so-called Constrained MSSM (CMSSM) [2].¹ In the CMSSM, at the GUT scale the soft masses of all the sleptons, squarks and Higgs bosons have a common scalar mass m_0 , all the gauginos unify at the common gaugino mass $m_{1/2}$, and so all the tri-linear terms assume a common tri-linear mass parameter A_0 . In addition, at the electroweak scale one selects $\tan\beta$, the ratio of Higgs vacuum expectation values and $\text{sign}(\mu)$, where μ is the Higgs/higgsino mass parameter whose square is computed from the conditions of radiative electroweak symmetry breaking (EWSB).

The small number of parameters makes the CMSSM a popular framework for exploring SUSY phenomenology. Conversely, collider data provides useful constraints on the parameter space (PS) of the CMSSM. In the presence of R-parity the lightest neutralino is often the lightest supersymmetric particle (LSP). Assuming it to be the dominant component of cold dark matter (DM) in the Universe, allows one to apply the DM relic density determination by WMAP and other experiments as a strong constraint on the CMSSM PS [4].

Another important constraint on the CMSSM comes from the process $b \rightarrow s\gamma$. An approximate agreement of the Standard Model (SM) prediction for $BR(\bar{B} \rightarrow X_s\gamma)$ with

¹One well-known implementation of the CMSSM is the minimal supergravity model [3].

an experimental determination requires the sum of SUSY contributions, which enter at the same 1-loop level, to be strongly suppressed. While the experimental world average has for over a year remained at $(3.55 \pm 0.26) \times 10^{-4}$ [5], the recently re-evaluated SM value of $BR(\bar{B} \rightarrow X_s \gamma)$, as obtained by Misiak et al., in [6, 7], has moved quite substantially from $(3.60 \pm 0.30) \times 10^{-4}$ down to $(3.15 \pm 0.23) \times 10^{-4}$.² The main shift was caused by including new partial NNLO SM contributions, most importantly an approximate evaluation of the charm mass effects. The new SM value leads to some discrepancy, at the level of 1.2σ , with the experimental average.

From the perspective of SUSY corrections, much more important than this slight discrepancy is the fact that the SM central value has now moved from above to below the experimental one. In the case of minimal flavor violation, which is applicable to the CMSSM, dominant SUSY contributions come from the charged Higgs/top loop, which always adds constructively to the SM contribution, and from the chargino/stop loops, whose sign is opposite to that of μ . With the previous SM value of the $b \rightarrow s\gamma$ branching ratio, this was used as an argument for assuming μ to be positive. Indeed, for $\mu < 0$ one had to push superpartner masses into the multi-TeV range in order for the chargino/stop loop correction to become suppressed, while in the opposite case much smaller masses were allowed. However, the recent shift in the SM predictions for $BR(\bar{B} \rightarrow X_s \gamma)$ makes the argument for selecting $\mu > 0$ questionable, and has in fact motivated us to perform this analysis.

Another argument that is often used in favor of $\mu > 0$ is based on a persistent discrepancy of $a_\mu^{\text{expt}} - a_\mu^{\text{SM}} = (28 \pm 8.1) \times 10^{-10}$ between the experimental value and the SM prediction of the anomalous magnetic moment of the muon $(g - 2)_\mu$ [9]. Taking the nearly 3.5σ difference as being due to SUSY contributions, $\delta a_\mu^{\text{SUSY}} \equiv a_\mu^{\text{expt}} - a_\mu^{\text{SM}}$, (whose sign is the same as that of μ), implies $\mu > 0$.

However, such conclusions are based on a somewhat oversimplified treatment of both theoretical and experimental uncertainties, which is common practice in fixed-grid scans of a SUSY PS. In such studies, a “step-function” approach is usually adopted: regions of the PS where contributions to a given observable are within the $\pm 1\sigma$ (or some other) range around the experimental central value are treated as fully allowed, while those even slightly outside are treated as completely ruled out. The same applies to experimental limits, e.g., on Higgs or superpartner masses. Instead, it seems more justified to assign varying “weights” to different points in a PS, depending on how well, or how poorly, a prediction for a given observable matches its experimental determination. Furthermore, in the usual approach theoretical errors are typically neglected, and so are residual uncertainties in relevant SM parameters, simply for the reason of practicality.

Recently a more refined procedure has been developed which allows one to overcome these shortcomings. It is based on a statistical Bayesian analysis linked with a Markov Chain Monte Carlo (MCMC) scanning techniques [10, 11], and is becoming increasingly popular in studying SUSY phenomenology [12–17]. The MCMC technique allows one

²A further slight decrease to $(2.98 \pm 0.26) \times 10^{-4}$ after including some additional partial effects due to a treatment of a photon energy cut $E_\gamma > 1.6$ GeV was obtained in ref. [8]. Note that the above values do depend on the choice of the cut in E_γ .

to make a thorough scan of a model's full multi-dimensional PS. Additionally maps of probability distributions can be drawn both for the model's parameters and also for all the observables (and their combinations) included in the analysis. In this approach, sharply defined "allowed regions" drawn up in fixed-grid scans are replaced by more informative probability distributions.

The MCMC Bayesian approach to studying properties of "new physics" models, like the CMSSM, is superior in the sense of treating the impact of different experimental data with their proper weights. It allows to make global scans of the PS and to derive its global properties and predictions. When (hopefully) discoveries are eventually made at current or future experiments, the approach will provide invaluable in assessing their implications for a given theoretical model.

In this work we apply the MCMC Bayesian formalism to explore the impact on the CMSSM's properties from mostly the recent change in the SM value for $BR(\overline{B} \rightarrow X_s \gamma)$. As we will see, regions of the highest posterior probability, will move rather dramatically to the focus point (FP) [18] region of the CMSSM PS. This in turn will lead to a significant shift in prospects for superpartner searches at the LHC (generally for worse) and in direct searches for DM neutralinos in the Milky Way (generally for better), while chances of finding h^0 at the Tevatron will remain good.

In order to assess the robustness of the results obtained in Bayesian language, following our previous work [14, 16] we also apply an alternative measure of a mean quality-of-fit, which is similar to a popular χ^2 -measure, which singles out (possibly limited) ranges of parameters that give the best fit to the data.

We consider both signs of μ . In the probabilistic approach, the case $\mu < 0$ cannot be treated anymore as ruled out, but merely as disfavored, by the $(g-2)_\mu$ result. The relative weight of this constraint has to be compared with that of other observables in a proper statistical way. In a recent similar study of Allanach et al., [15] (although done with the old values of $BR(\overline{B} \rightarrow X_s \gamma)$ and $\delta a_\mu^{\text{SUSY}}$) fits for both signs of μ were performed. It was concluded that the the case $\mu < 0$ was only marginally disfavored, with the ratio of probabilities estimated at $P(\mu < 0)/P(\mu > 0) = 0.07-0.16$. In our study we also find that the case of $\mu < 0$ gives a worse fit to the data than the opposite sign of μ , although the level of preference for $\mu > 0$ is difficult to quantify. On the other hand, unlike in [15], we are not interested in comparing the relative probabilities of the two cases $\mu < 0$ and $\mu > 0$, but rather emphasize different implications of each one for various observables of interest.

In this paper we include, and update when applicable, all relevant experimental constraints from collider direct searches and from rare processes, and also from cosmology on the relic abundance of the lightest neutralino $\Omega_\chi h^2$. We further take into account residual error bars in relevant SM parameters. Details of our analysis will be given below.

We adopt flat priors on the usual CMSSM parameters: $m_{1/2}$, m_0 , A_0 and $\tan \beta$. We do this primarily for the sake of comparing our results with the literature (in particular with the fixed-grid scan approach) where this parametrization is usually assumed. Some of our specific results will accordingly depend on this choice, as we discuss later.

Implications from the current analysis (assuming $\mu > 0$) for the Higgs bosons have already been presented in [16] where we showed that, with our choice of priors, the light-

est Higgs boson h^0 mass is confined to $115.4 \text{ GeV} < m_h < 120.4 \text{ GeV}$ (95% probability interval) and that its couplings to electroweak gauge bosons are very close to those of the SM Higgs boson with the same mass. This range should be excluded (at 95% CL) at the Tevatron. Here we extend our analysis to the case $\mu < 0$, reaching similar conclusions for h^0 at the Tevatron. We also derive most probable ranges of several sparticle masses, of the rates of rare bottom quark processes, and of both spin-independent and spin-dependent cross sections for dark matter neutralino scattering off nuclei.

The paper is organized as follows. In section 2 we outline our theoretical setup. In section 3 we present our numerical results for the PS of the CMSSM in terms of the Bayesian statistics and of the mean quality-of-fit, and resulting implications for several observables. We finish with summary and conclusions in section 4.

2. The analysis

Our procedure based on MCMC scans and Bayesian analysis has been presented in detail in [14]. Here, for completeness, we repeat its main features following an updated presentation given in [16].

2.1 Theoretical framework

In the CMSSM the parameters $m_{1/2}$, m_0 and A_0 , which are specified at the GUT scale $M_{\text{GUT}} \simeq 2 \times 10^{16} \text{ GeV}$, serve as boundary conditions for evolving, for a fixed value of $\tan \beta$, the MSSM Renormalization Group Equations (RGEs) down to a low energy scale $M_{\text{SUSY}} \equiv \sqrt{m_{\tilde{t}_1} m_{\tilde{t}_2}}$ (where $m_{\tilde{t}_1, \tilde{t}_2}$ denote the masses of the scalar partners of the top quark), chosen so as to minimize higher order loop corrections. At M_{SUSY} the (1-loop corrected) conditions of electroweak symmetry breaking (EWSB) are imposed and the SUSY spectrum is computed at m_Z .

We are interested in delineating high probability regions of the CMSSM parameters. We consider separately both signs of μ and denote the remaining four free CMSSM parameters by the set

$$\theta = (m_0, m_{1/2}, A_0, \tan \beta). \tag{2.1}$$

As demonstrated in [12, 14], the values of the relevant SM parameters can strongly influence some of the CMSSM predictions, and, in contrast to common practice, should not be simply kept fixed at their central values. We thus introduce a set ψ of so-called “*nuisance parameters*” of those SM parameters which are relevant to our analysis,

$$\psi = (M_t, m_b(m_b)^{\overline{MS}}, \alpha_{\text{em}}(M_Z)^{\overline{MS}}, \alpha_s(M_Z)^{\overline{MS}}), \tag{2.2}$$

where M_t is the pole top quark mass. The other three parameters: $m_b(m_b)^{\overline{MS}}$ — the bottom quark mass evaluated at m_b , $\alpha_{\text{em}}(M_Z)^{\overline{MS}}$ and $\alpha_s(M_Z)^{\overline{MS}}$ — respectively the electromagnetic and the strong coupling constants evaluated at the Z pole mass M_Z - are all computed in the \overline{MS} scheme.

The set of parameters θ and ψ form an 8-dimensional set m of our “*basis parameters*” $m = (\theta, \psi)$.³ In terms of the basis parameters we compute a number of collider and

³In [14] we denoted our basis parameters with a symbol η .

cosmological observables, which we call “*derived variables*” and which we collectively denote by the set $\xi = (\xi_1, \xi_2, \dots)$. The observables, which are listed below, will be used to compare CMSSM predictions with a set of experimental data d , which is available either in the form of positive measurements or as limits.

In order to map out high probability regions of the CMSSM, we compute the *posterior probability density functions* (pdf’s) $p(m|d)$ for the basis parameters m and for several observables. The posterior pdf represents our state of knowledge about the parameters m after we have taken the data into consideration. Using Bayes’ theorem, the posterior pdf is given by

$$p(m|d) = \frac{p(d|\xi)\pi(m)}{p(d)}. \tag{2.3}$$

On the r.h.s. of eq. (2.3), the quantity $p(d|\xi)$, taken as a function of ξ for *fixed data* d , is called the *likelihood* (where the dependence of $\xi(m)$ is understood). The likelihood supplies the information provided by the data and, for the purpose of our analysis, it is constructed in section 3.1 of ref. [14]. The quantity $\pi(m)$ denotes a *prior probability density function* (hereafter called simply *a prior*) which encodes our state of knowledge about the values of the parameters in m before we see the data. The state of knowledge is then updated to the posterior via the likelihood. Finally, the quantity in the denominator is called *evidence* or *model likelihood*. Here it only serves a normalization constant, independent of m , and therefore will be dropped in the following. As in ref. [14], our posterior pdf’s presented below will be normalized to their maximum values, and *not* in such a way as to give a total probability of 1. Accordingly we will use the name of a “relative posterior pdf”, or simply of “relative probability density”.

The Bayesian approach to parameter inference relies on the updating of the prior probability to the posterior through the information provided by the data (via the likelihood). This requires specification of the prior probabilities for the parameters of the model, that in our case are taken to be flat (i.e., constant) over a large range of the CMSSM and SM parameters given above. If the data are not strongly constraining, the choice of prior can lead to a significant impact through the effect of the “volume” of the parameter space. Indeed, as we discussed in ref. [14], imagine the situation that there exist a rather large region of the PS where theoretical predictions match the data rather well. In addition, let there be a rather small, possibly fined-tuned, region giving very good match of the data. The Bayesian posterior probability would give an overwhelming weight to the larger region, due to the much larger volume it occupies in parameter space. We notice that this kind of situation only arises in the “grey zone” of insufficient data, since of course if the data were powerful enough as to rule out such a large region, then the Bayesian posterior probability would show this by peaking in correspondence with the best fitting, smaller region. As done previously in refs. [14, 16], we therefore consider also an alternative statistical measure of the mean quality-of-fit defined in [14], which is much more sensitive to possibly small best-fit regions. Below we will compare results obtained using the two measures.

2.2 Constraints

We perform a scan over very wide ranges of CMSSM parameters [14, 16]. In particular we

SM (nuisance) parameter	Mean value μ	Uncertainty σ (exper.)	ref.
M_t	171.4 GeV	2.1 GeV	[19]
$m_b(m_b)^{\overline{MS}}$	4.20 GeV	0.07 GeV	[9]
$\alpha_s(M_Z)^{\overline{MS}}$	0.1176	0.002	[9]
$1/\alpha_{\text{em}}(M_Z)^{\overline{MS}}$	127.955	0.018	[9]

Table 1: Experimental mean μ and standard deviation σ adopted for the likelihood function for SM (nuisance) parameters, assumed to be described by a Gaussian distribution.

take flat priors on the ranges $50 \text{ GeV} < m_{1/2}, m_0 < 4 \text{ TeV}$ (this way including the focus point region), $|A_0| < 7 \text{ TeV}$ and $2 < \tan \beta < 62$. For the SM (nuisance) parameters, we assume flat priors over wide ranges of their values [14] and adopt a Gaussian likelihood with mean and standard deviation as given in table 1. Note that, with respect to ref. [14], we have updated the values of all the constraints.⁴

The experimental values of the collider and cosmological observables that we apply (our derived variables) are listed in table 2, with updates where applicable. In our treatment of the radiative corrections to the electroweak observables M_W and $\sin^2 \theta_{\text{eff}}$, starting from ref. [16] we include full two-loop and known higher order SM corrections as computed in ref. [26], as well as gluonic two-loop MSSM corrections obtained in [27]. We further update an experimental constraint from the anomalous magnetic moment of the muon $(g - 2)_\mu$ for which a discrepancy (denoted by $\delta a_\mu^{\text{SUSY}}$) between measurement and SM predictions (based on e^+e^- data) persists at the level of 3.5σ [9]. We note here, however, that the impact of this (still somewhat uncertain) constraint on our findings will be rather limited because the corresponding error bar remains relatively large.⁵

As regards $BR(\overline{B} \rightarrow X_s \gamma)$, with the central values of SM input parameters as given in table 1, for the new SM prediction we obtain the value of $(3.11 \pm 0.21) \times 10^{-4}$.⁶ We compute SUSY contribution to $BR(\overline{B} \rightarrow X_s \gamma)$ following the procedure outlined in refs. [29, 30] which were extended in refs. [31, 32] to the case of general flavor mixing. In addition to full leading order corrections, we include large $\tan \beta$ -enhanced terms arising from corrections coming from beyond the leading order and further include (subdominant) electroweak corrections.

Regarding cosmological constraints, we use the determination of the relic abundance of

⁴After completing our numerical scans, a new value of the top mass, $M_t = 170.9 \pm 1.8 \text{ GeV}$, based on Tevatron's Run-II 1 fb^{-1} of data was released [20]. Including it would not have much impact on our results, since the shift in the mean value of M_t is very mild if compared to the standard deviation adopted in this paper.

⁵Although the different evaluations seem to be converging; e.g., recently $(27.6 \pm 8.1) \times 10^{-10}$ was obtained in ref. [28].

⁶The value of $(3.15 \pm 0.23) \times 10^{-4}$ originally derived in ref. [6, 7] was obtained for slightly different values of M_t and $\alpha_s(M_Z)^{\overline{MS}}$. Note that, in treating the error bar we have explicitly taken into account the dependence on M_t and $\alpha_s(M_Z)^{\overline{MS}}$, which in our approach are treated parametrically. This has led to a slight reduction of its value. Note also that even though the theoretical error is, strictly speaking, not Gaussian, it can still be approximately treated as such as it represents an estimate where a larger assumed error of the (dominant) uncertainty due to non-perturbative effects is assigned lower probability - M. Misiak, private communication.

Observable	Mean value	Uncertainties		ref.
	μ	σ (exper.)	τ (theor.)	
M_W	80.392 GeV	29 MeV	15 MeV	[21]
$\sin^2 \theta_{\text{eff}}$	0.23153	16×10^{-5}	15×10^{-5}	[21]
$\delta a_\mu^{\text{SUSY}} \times 10^{10}$	28	8.1	1	[9]
$BR(\overline{B} \rightarrow X_s \gamma) \times 10^4$	3.55	0.26	0.21	[5]
ΔM_{B_s}	17.33 ps ⁻¹	0.12 ps ⁻¹	4.8 ps ⁻¹	[22]
$\Omega_\chi h^2$	0.104	0.009	$0.1 \Omega_\chi h^2$	[23]
	Limit (95% CL)		τ (theor.)	ref.
$BR(\overline{B}_s \rightarrow \mu^+ \mu^-)$	$< 1.0 \times 10^{-7}$		14%	[24]
m_h	> 114.4 GeV (91.0 GeV)		3 GeV	[25]
ζ_h^2	$f(m_h)$		negligible	[25]
sparticle masses	See table 4 in ref. [14].			

Table 2: Summary of the observables used in the analysis. Upper part: Observables for which a positive measurement has been made. $\delta a_\mu^{\text{SUSY}} = a_\mu^{\text{expt}} - a_\mu^{\text{SM}}$ denotes the discrepancy between the experimental value and the SM prediction of the anomalous magnetic moment of the muon $(g-2)_\mu$. For central values of the SM input parameters used here, the SM value of $BR(\overline{B} \rightarrow X_s \gamma)$ is 3.11×10^{-4} , while the theoretical error of 0.21×10^{-4} includes uncertainties other than the parametric dependence on the SM nuisance parameters, especially on M_t and $\alpha_s(M_Z)^{\overline{MS}}$. As explained in the text, for each quantity we use a likelihood function with mean μ and standard deviation $s = \sqrt{\sigma^2 + \tau^2}$, where σ is the experimental uncertainty and τ represents our estimate of the theoretical uncertainty. Lower part: Observables for which only limits currently exist. The likelihood function is given in ref. [14], including in particular a smearing out of experimental errors and limits to include an appropriate theoretical uncertainty in the observables. m_h stands for the light Higgs mass while $\zeta_h^2 = g^2(hZZ)_{\text{MSSM}}/g^2(hZZ)_{\text{SM}}$, where g stands for the Higgs coupling to the Z and W gauge boson pairs.

cold DM based on the 3-year data from WMAP [23] to constrain the relic abundance $\Omega_\chi h^2$ of the lightest neutralino which we compute with high precision, including all resonance and coannihilation effects, as explained in ref. [14], and solve the Boltzmann equation numerically as in ref. [33]. In order to remain on a conservative side, we impose the following Gaussian distribution

$$\Omega_\chi h^2 = 0.104 \pm \sqrt{(0.009)^2 + (0.1 \Omega_\chi h^2)^2} = 0.104 \pm 0.009 \sqrt{1 + 1.335 (\Omega_\chi h^2 / 0.104)^2} \quad (2.4)$$

Note that our estimated theoretical uncertainty is of the same order as the uncertainty from current cosmological determinations of $\Omega_{\text{CDM}} h^2$.

We further include in our likelihood function an improved 95% CL limit on $BR(\overline{B}_s \rightarrow \mu^+ \mu^-)$ and a recent value of \overline{B}_s - B_s mixing, ΔM_{B_s} , which has recently been precisely measured at the Tevatron by the CDF Collaboration [22]. In both cases we use expressions from ref. [32] which include dominant large $\tan \beta$ -enhanced beyond-LO SUSY contributions from Higgs penguin diagrams. Unfortunately, theoretical uncertainties, especially in lattice evaluations of f_{B_s} are still very large (as reflected in table 2 in the estimated theoretical error for ΔM_{B_s}), which makes the impact of this precise measurement on constraining the

CMSSM parameter space rather limited.⁷

For the quantities for which positive measurements have been made (as listed in the upper part of table 2), we assume a Gaussian likelihood function with a variance given by the sum of the theoretical and experimental variances, as motivated by eq. (3.3) in ref. [14]. For the observables for which only lower or upper limits are available (as listed in the bottom part of table 2) we use a smoothed-out version of the likelihood function that accounts for the theoretical error in the computation of the observable, see eq. (3.5) and figure 1 in [14]. In applying the Higgs boson h^0 lower mass bounds from LEP-II we take into account its dependence on its coupling to the Z boson pairs $\zeta_h^2 \equiv g^2(hZZ)_{\text{MSSM}}/g^2(hZZ)_{\text{SM}}$, as described in detail in ref. [16]. When $\zeta_h^2 \simeq 1$, the LEP-II lower bound of 114.4 GeV (95% CL) [25] is applicable. For arbitrary values of ζ_h , we apply the LEP-II 95% CL bounds on m_h and m_A , which we translate into the corresponding 95% CL bound in the (m_h, ζ_h^2) plane. We then add a theoretical uncertainty $\tau(m_h) = 3$ GeV, following eq. (3.5) in ref. [14]. However, a posteriori we find $\zeta_h^2 \simeq 1$ which means that the CMSSM light Higgs boson is invariably SM-like. This procedure results in a conservative likelihood function for m_h , which does not simply cut away points below the 95% CL limit of LEP-II, but instead assigns to them a lower probability that gradually goes to zero for lower masses.

Finally, points that do not fulfil the conditions of radiative EWSB and/or give non-physical (tachyonic) solutions are discarded. We adopt the same convergence and mixing criteria as described in appendix A2 of ref. [14], while our sampling procedure is described in appendix A1 of ref. [14]. We have the total of $N = 10$ MC chains, with a merged number of samples 2×10^5 , and an acceptance rate of about 1.5%. We adopt the Gelman & Rubin mixing criterion, with the inter-chain variance divided by the intra-chain variance (the $R - 1$ parameter) being less than 0.1 along all directions in parameter space. More details of our numerical MCMC scan can be found in [14].

3. Results

We will now explore the implications of the above constraints on the CMSSM parameters, paying particular attention to the impact of $BR(\overline{B} \rightarrow X_s \gamma)$. We will compare the posterior probability distributions of the Bayesian language with the ranges favored by the mean quality-of-fit. Next, we will discuss implications for Higgs and superpartner masses and for direct detection of the neutralino dark matter. In computing the Higgs (and SUSY) mass spectrum we employ the code SOFTSUSY v2.08 [35]. The results presented in this paper are obtained using a new publicly available package, called SuperBayeS, available from superbayes.org.

3.1 Implications for the CMSSM parameters

We first show in figure 1 the 2-dim relative probability density functions in the planes spanned by the CMSSM parameters: $m_{1/2}$, m_0 , $\tan \beta$, A_0 , and assuming $\mu > 0$, while

⁷On the other hand, in the MSSM with general flavor mixing, even with the current theoretical uncertainties, the bound from ΔM_{B_s} is in many cases much more constraining than from other rare processes [34].

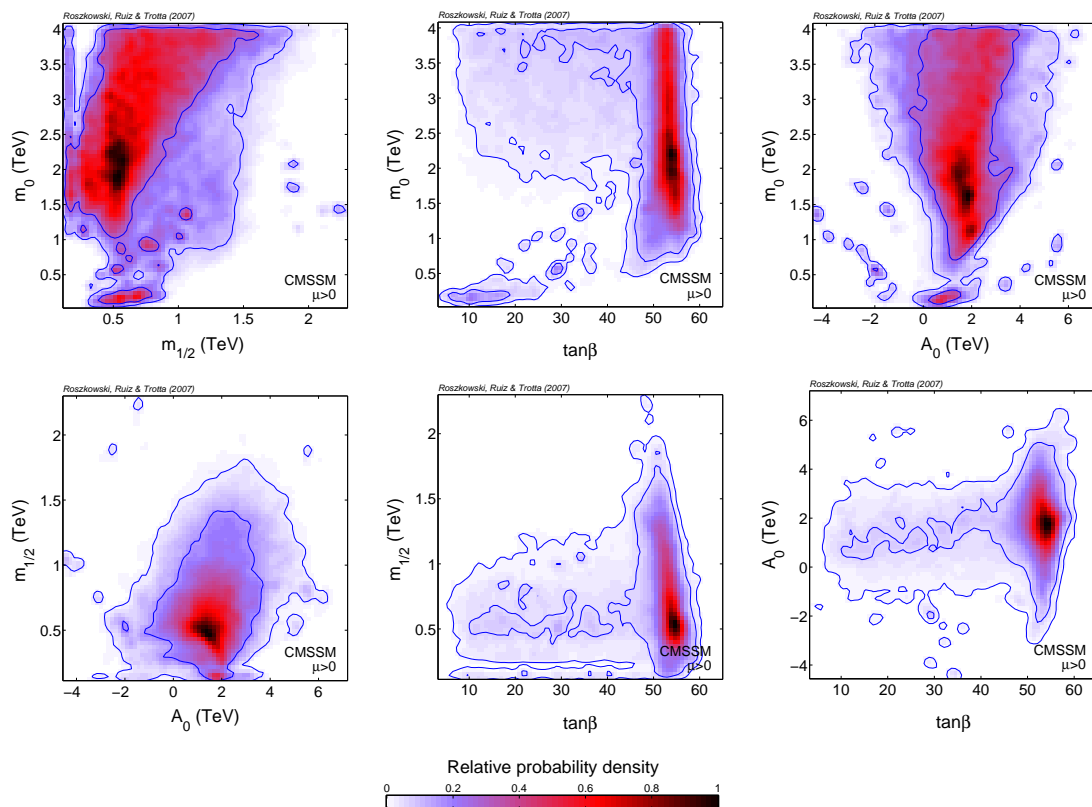


Figure 1: The 2-dim relative probability density functions in the planes spanned by the CMSSM parameters: $m_{1/2}$, m_0 , A_0 and $\tan\beta$ for $\mu > 0$. The pdf's are normalized to unity at their peak. The inner (outer) blue solid contours delimit regions encompassing 68% and 95% of the total probability, respectively. All other basis parameters, both CMSSM and SM ones, in each plane have been marginalized over. This figure should be compared with figure 2 in ref. [14].

in figure 2 the same is shown for $\mu < 0$. In each panel all other basis parameters have been marginalized over. Redder (darker) regions correspond to higher probability density. Inner and outer blue (dark) solid contours delimit regions of 68% and 95% of the total probability, respectively, and remain well within the assumed priors, except for m_0 . In all the 2-dim plots, the MC samples have been divided into 70×70 bins, with a mild smoothing across adjacent bins to improve the quality of the presentation (this has no impact on our statistical conclusions). Jagged contours are a result of a finite resolution of the MC chains.

In the case of $\mu > 0$ (figure 1) we can see a strong preference for large $m_0 \gtrsim 1$ TeV. On the other hand, the peak of probability for $m_{1/2}$ is around 0.5 TeV, although the 68% range of total probability is rather wide, increases with m_0 and exceeds 1.5 TeV for $m_0 \simeq 4$ TeV. Additionally, at smaller $m_0 \lesssim 1$ TeV there are a few confined 68% total probability regions.

The strong preference for large $m_0 \gg m_{1/2}$ is primarily the result of the sizable shift in the SM value of $BR(\bar{B} \rightarrow X_s \gamma)$, as can be seen by comparing figure 1 with figure 2 in ref. [14] (or figure 8 of ref. [15]) where the previous value of $BR(\bar{B} \rightarrow X_s \gamma)$ has been used. (While the other CMSSM parameters also experience some shift in their most probable

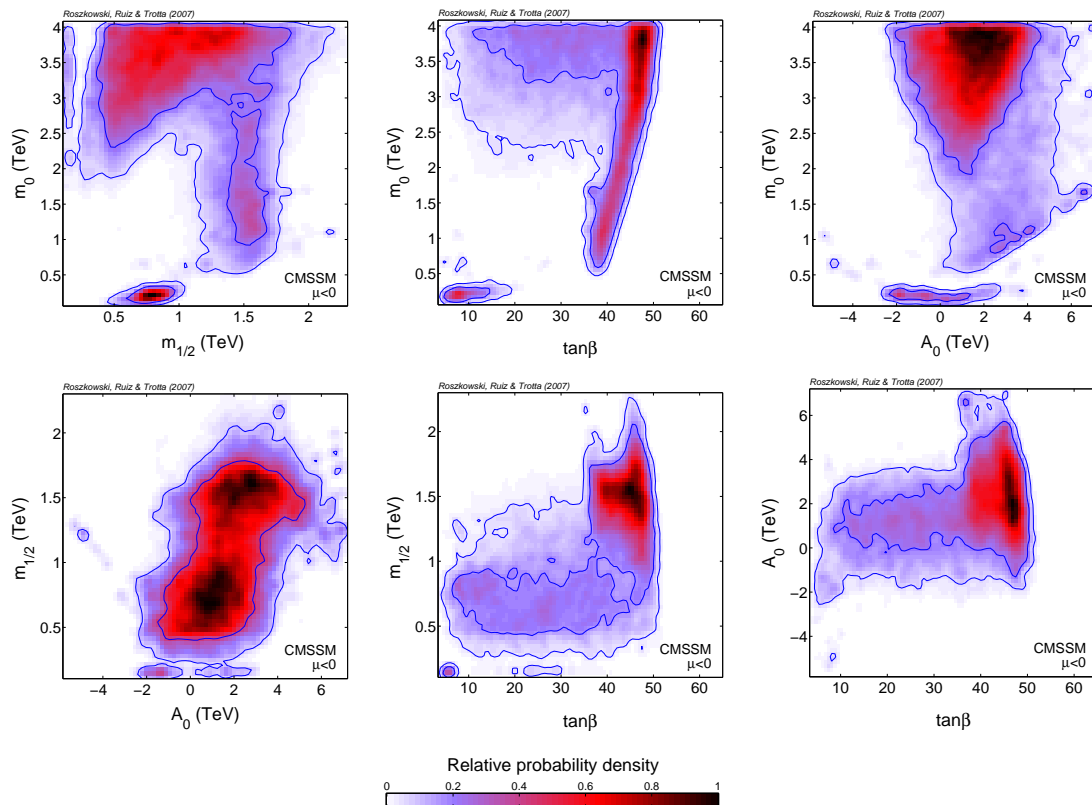


Figure 2: The same as in figure 1 but for $\mu < 0$.

values, it is not as dramatic as that of m_0 towards larger values.) The underlying reason is that, at fairly small $m_{1/2}$ the charged Higgs mass remains relatively light, in the few hundred GeV range, and, via a loop exchange with the top quark, it adds substantially to the SM value of $BR(\overline{B} \rightarrow X_s \gamma)$, towards the experimentally allowed range. (In fact, for $m_{H^-} \simeq 650$ GeV, the contribution is sufficient to fill the gap between the SM and the experimental central values of $BR(\overline{B} \rightarrow X_s \gamma)$ [6].) At smaller $m_{1/2}$ and/or m_0 , the (negative, for $\mu > 0$) chargino-stop contribution is too large and needs to be compensated by the H^- -top contribution. In fact, we do find some small “islands” of 68% total probability at $m_{1/2} \lesssim 1$ TeV and $m_0 \lesssim 1.3$ TeV (in particular, notably, an interesting case of $m_{1/2} \simeq 0.5$ TeV and $m_0 \simeq 0.2$ TeV) but the bulk of high probability region corresponds to $m_0 \gtrsim 1$ TeV.

At 95% total probability level the available parameter space widens considerably, and also some new features arise. In particular, at $m_{1/2} \simeq 0.2$ TeV we can see a narrow high-probability funnel induced by the light Higgs boson resonance [12, 14]. Also, $\tan \beta$ becomes less confined to its most preferred range of large values between some 50 and 60, while A_0 remains on a positive side.

In the case of $\mu < 0$ (figure 2), one can see a strong preference for even larger m_0 . Also, the 68% total probability region of $m_{1/2}$ shifts towards larger values, although still remains

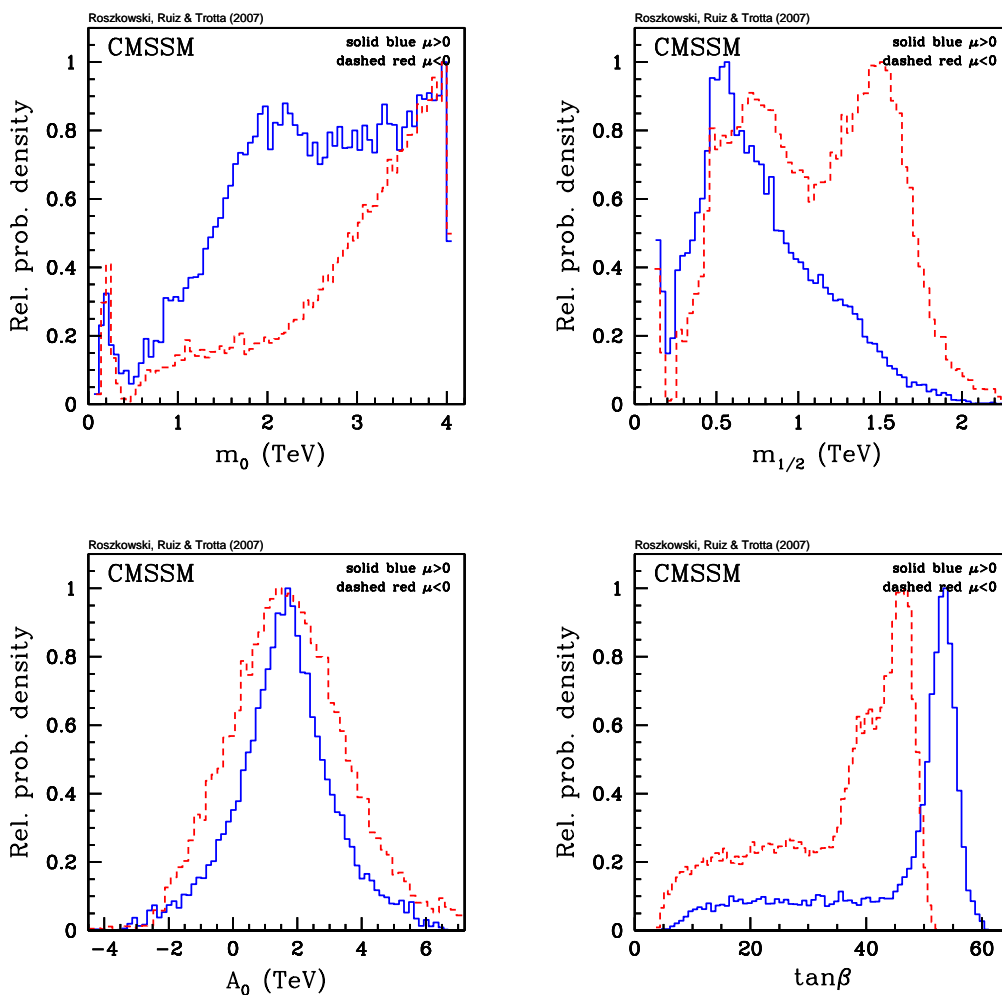


Figure 3: The 1-dim relative probability densities for the CMSSM parameters m_0 , $m_{1/2}$, A_0 and $\tan\beta$. All other parameters have been marginalized over. Solid blue (dashed red) curves correspond to $\mu > 0$ ($\mu < 0$). This figure should be compared with figure 4 (black solid lines) in ref. [14].

basically below 2 TeV. (Although we again find an interesting isolated high probability region at $m_{1/2} \simeq 0.75$ TeV and $m_0 \simeq 0.2$ TeV.) This shift towards larger m_0 and/or $m_{1/2}$ is again caused mostly by the $BR(\bar{B} \rightarrow X_s \gamma)$ constraint. At large m_0 (and not too large $m_{1/2}$) the charged Higgs mass *decreases* and its contribution tends to be on a high side, while the chargino-stop one becomes too small. A similar effect is observed at large $m_{1/2} \sim 1.5$ TeV and $m_0 \gtrsim 1$ TeV where the chargino and stop masses become too large to contribute much as well.

In figure 3 the 1-dim marginalized probability distributions for the CMSSM parameters are compared for both $\mu > 0$ and $\mu < 0$. In each panel all the other CMSSM parameters and all SM (nuisance) parameters have been marginalized over. It is clear that non-negligible probability ranges of the CMSSM parameters, other than m_0 , are confined well within their

assumed priors. Again, we can see strong preference for large $m_0 \gg 1$ TeV (even stronger for $\mu < 0$ than for $\mu > 0$). Larger values of $m_{1/2}$ are also favored for $\mu < 0$ although, for both signs, this parameter is well confined within 2 TeV. The preferred range of A_0 is fairly uncorrelated with the other parameters [14], and it is symmetrically peaked (basically independently of the sign of μ) at some 1.5 TeV. This value is however basically twice as large as for the previous SM value of $BR(\bar{B} \rightarrow X_s \gamma)$ [14]. On the other hand, $\tan \beta$ is well-peaked at some 53 for $\mu > 0$ and some 48 for $\mu < 0$. In both cases, there remains a sizable tail of much smaller values which remain allowed at large m_0 .

What most strongly contributes to confining $m_{1/2}$ well within its prior (for both signs of μ) is the relic abundance $\Omega_\chi h^2$ which becomes too large for large $m_{1/2}$. On the one hand, at large $\tan \beta$ it becomes easier to satisfy the constraint from $\Omega_\chi h^2$ due to the increased role of the neutralino annihilation via the pseudoscalar Higgs effect and/or the coannihilation effect. On the other, as explained in ref. [14, 16], as $\tan \beta$ becomes very large, $\gtrsim 60$ for $\mu > 0$ ($\gtrsim 50$ for $\mu < 0$), it becomes very difficult to find self-consistent solutions of the RGE's.

The feature that very large values of m_0 (the FP region), up to the assumed prior of 4 TeV, remain allowed (actually, even preferred), is unfortunate but is a consequence of the fact that current data are not constraining enough. Normally, as all the superpartner masses (including the LSP) increase, bino-like neutralino annihilation in the early Universe becomes suppressed and it becomes harder to satisfy the WMAP constraint on $\Omega_\chi h^2$. This is why $m_{1/2}$ is well confined within some 2 TeV, as described above. Unfortunately, in the FP region the behavior of $\Omega_\chi h^2$ is much more sensitive to input parameters. We illustrate this in figure 4 where we plot $\Omega_\chi h^2$ vs. m_0 for $\mu > 0$ and a choice of the other CMSSM parameters close to their highest probability values (figure 1). Clearly, as M_t is varied within 1σ around its central value (cv), $\Omega_\chi h^2$ changes quite substantially. In the presented example, by fixing M_t at its central value [36] (as it is normally done in fixed-grid scans) one would find no cosmologically allowed m_0 . On the other hand, by reducing (increasing) M_t by 1σ we can find one (two widely disconnected) narrow region(s) of m_0 where $\Omega_\chi h^2$ in the WMAP range. Furthermore, in a probabilistic approach, even the case at the central value of M_t is not excluded but only less favored by $\Omega_\chi h^2$.

Another feature that is evident in figure 4 is that, as M_t is varied by 1σ around its central value, the range of m_0 where self-consistent solutions of the RGE's and the conditions of EWSB can be found changes by as much as a factor of two. It is therefore clear that, if one includes the FP region, it is basically impossible to locate the cosmologically favored range of m_0 . In particular, it would be misleading to simply fix the top mass at its central value (and likewise with the bottom mass at large $\tan \beta$).

The rather special properties of the FP region are to a large extent related to the behavior of the parameter μ . As m_0 increases (along, say, fixed $m_{1/2}$), μ^2 (which is determined the conditions of EWSB) decreases rather quickly, thus increasing the higgsino component of the neutralino. This in turn reduces $\Omega_\chi h^2$ to an acceptable range for some narrow range of m_0 . At slightly larger m_0 , μ^2 drops below zero, thus delimiting the zone where consistent, non-tachyonic solutions can be found. Thus generally in the FP region μ is rather small relative to m_0 . We can see this feature in figure 5 where we plot the

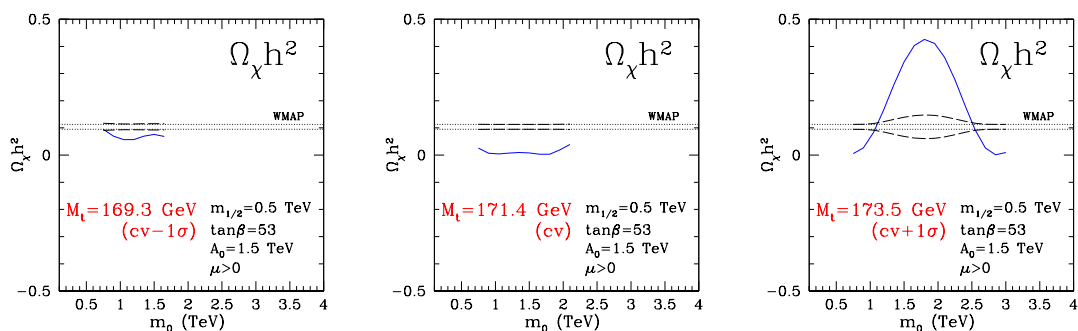


Figure 4: An illustration of the sensitivity of the cosmologically favored range of m_0 to the top mass M_t in the focus point region. Other CMSSM parameters have been fixed close to their most preferred values for $\mu > 0$ (see figure 1). We show $\Omega_\chi h^2$ (blue solid line) for the central value (cv) of M_t (middle panel) and for the values decreased and increased by 1σ (left and right panel). The parallel dotted lines denote the very narrow 2σ range, as determined from the 3-year data of WMAP [23]. The long-dashed line denotes the combined theoretical plus experimental error, as described in the text. Note that, as M_t is varied between its cv minus 1σ to its cv plus 1σ , the range of m_0 , for which consistent solutions can be found, roughly doubles.

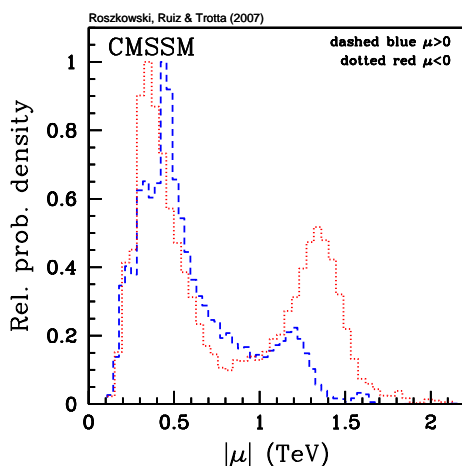


Figure 5: The 1-dim relative probability density of $|\mu|$. All other parameters have been marginalized over. Dashed blue (dotted red) curves correspond to $\mu > 0$ ($\mu < 0$).

1-dim relative probability density for the parameter. We can see a clear peak in the few hundred GeV region for both signs of μ . In this region $|\mu| \simeq m_{1/2}/3$. Additionally, for $\mu < 0$ there is a second well-pronounced peak around some 1.4 TeV which corresponds to the band of higher relative probability around $m_{1/2} \simeq 1.5$ TeV and $m_0 \gtrsim 1$ TeV in figure 2, outside of the FP region.

In order to summarize the above discussion, in table 3 we give the 68% and 95% total probability ranges of the CMSSM parameters for both signs of μ .

Parameter	$\mu < 0$		$\mu > 0$	
	68% region	95% region	68% region	95% region
m_0 (TeV)	< 3.51	< 3.93	< 3.1	< 3.87
$m_{1/2}$ (TeV)	(0.87, 1.55)	(0.57, 1.86)	(0.4, 1.16)	(0.14, 1.6)
A_0 (TeV)	(-0.19, 3.42)	(-1.79, 5.49)	(0.11, 2.94)	(-1.86, 4.84)
$\tan \beta$	(18.6, 46.08)	(7.51, 48.9)	(26.38, 54.18)	(11.17, 56.78)

Table 3: CMSSM parameter ranges corresponding to 68% and 95% of posterior probability (with all other parameters marginalized over) for both signs of μ .

We emphasize that the above results do not at all imply that it is equally easy to fit all the data for both signs of μ . (In figures 1–3 the posterior probabilities are normalized *relative* to the respective highest values.) Actually, for negative μ the fit is considerably poorer. In fact, we find that the best-fit χ^2 for the $\mu > 0$ case is 6.3, while for the $\mu < 0$ case it more than doubles to 14.4. It is difficult to attach a precise statistical significance to this result, as clearly the distributional properties of the parameter space are far from being Gaussian (and hence the χ^2 is not chi-square distributed). A proper evaluation of the significance of this difference in the goodness-of-fit would require Monte Carlo simulations of the measurements for both the $\mu > 0$ and $\mu < 0$ cases, which is beyond the scope of this work. However, this is an indication of the fact that the $\mu < 0$ case is at greater tension with the data than $\mu > 0$, although it cannot be conclusively ruled out yet.

A fully Bayesian approach would consider computing the Bayes factor among the two possibilities for μ , along the lines of what has been done in ref. [15]. This procedure is, however, computationally demanding, and the result is potentially strongly dependent on volume effects deriving from the choice of priors (see, eg., ref. [37]). An interesting alternative is to use the procedure outlined in ref. [38] which employs Bayesian calibrated p-values to obtain an upper limit on the Bayes factor regardless of the prior for the alternative hypothesis. In the present case, the application of this procedure would require Monte Carlo simulation to obtain the p-value corresponding to the observed χ -square difference. However, if we take again the result of $\Delta\chi^2 = 8$ at face value, assuming that it is indeed χ -square distributed (which is probably a very poor approximation, as argued above), then the corresponding upper limit on the Bayes factor is 16 : 1. (This rough estimate is actually in surprising good agreement with the result found in ref. [15] using numerical integrations) This would mean that the minimum probability of $\mu < 0$ is 6%, which certainly does not constitute strong evidence against $\mu < 0$. The above considerations only highlight the difficulty of translating our result into a precise statement about the relative probability of $\mu > 0$ vs $\mu < 0$.

A related (although somewhat different) issue is to identify regions of the CMSSM PS where the fit to the data is much better than elsewhere. As stated above, if such regions occupy a small volume of parameter space (given our choice of priors), the posterior pdf will consequently weight them down, although they might exhibit a higher goodness-of-fit. To address this point, we consider an alternative measure of the mean quality-of-fit, which

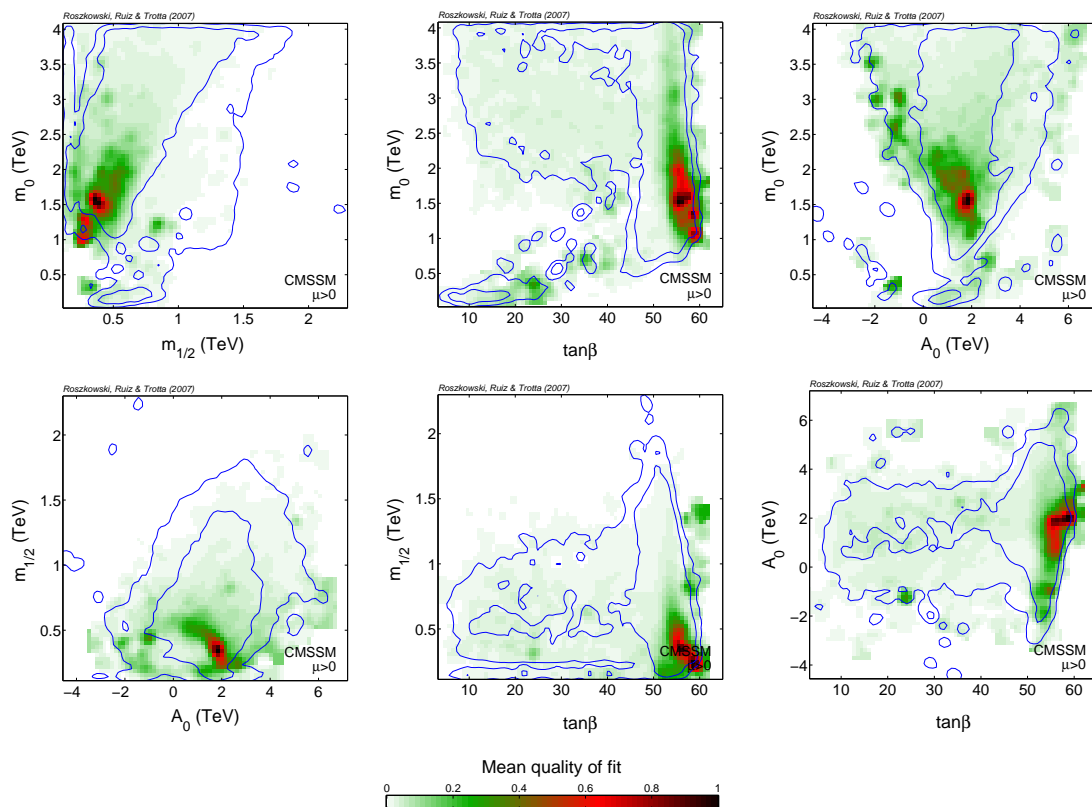


Figure 6: The mean quality-of-fit in the planes spanned by the CMSSM parameters: $m_{1/2}$, m_0 , A_0 and $\tan\beta$ for $\mu > 0$. For comparison, (blue solid) total posterior probability contours of 68% and 95% from figure 1 have been added. This figure should be compared with figure 11 in ref. [14].

is defined as the average of the effective χ^2 under the posterior distribution, i.e.,

$$\left\langle \exp\left(-\frac{\Delta\chi^2}{2}\right) \right\rangle = \int dm \exp\left(-\frac{\chi^2 - \chi_{\min}^2}{2}\right) p(m|d) \quad (3.1)$$

which is a quantity that is largely insensitive to the choice of priors (as long as the best-fitting points are explored by the MCMC scan). Its distribution for the CMSSM parameters is plotted in figures 6 and 7 for $\mu > 0$ and $\mu < 0$, respectively, in each case they are normalized to the respective best-fit value. We can see that, for $\mu > 0$, there indeed exists at least one well-localized region around $m_{1/2} \simeq 0.4$ TeV and $m_0 \simeq 1.5$ TeV (not far from the location of the highest relative pdf, and in any case within the 68% total probability contour), with another one at somewhat smaller values of both $m_{1/2}$ and m_0 . (Below we will show however that such best-fit regions may be in conflict with dark matter search limits, which have not been applied as constraints at this stage.) On the other hand, for $\mu < 0$ it is generally more difficult to find a good fit to the data, as indicated by the larger value of the χ^2 given above. We also notice that many of the best-fitting regions for the case $\mu < 0$ in figure 7 lie outside the 95% posterior probability contour, further indicating a strong tension with the data.

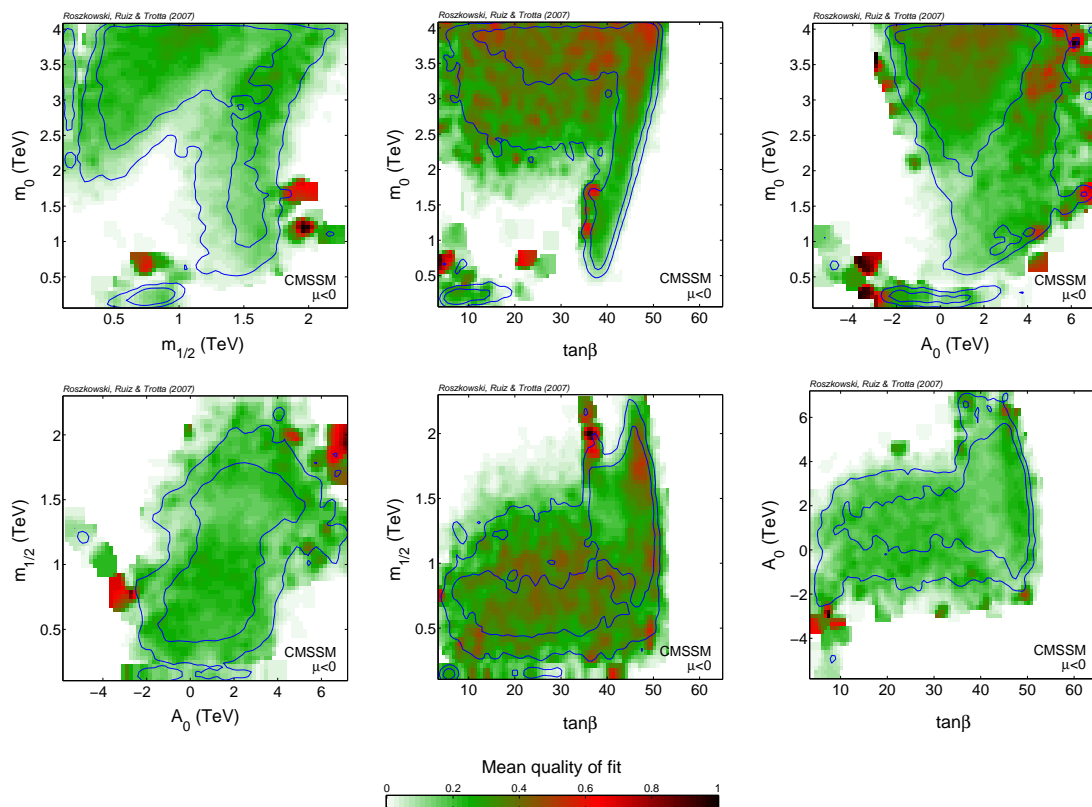


Figure 7: The same as in figure 6 but for $\mu < 0$. For comparison, (blue solid) total posterior probability contours of 68% and 95% from figure 2 have been added.

Different experimental observables may constrain or favor different regions of the CMSSM parameters; they may “pull” in different directions. We display this in figure 8 where we plot the 1-dim posterior pdf’s for several variables for both signs of μ . For comparison, we also plot the corresponding Gaussian likelihood functions representing the data used in the fit. If there was no tension among different observables then, in the absence of strong correlations among them, the relative probability curves should overlap with the data. This is basically the case for M_t , $\alpha_s(M_Z)^{\overline{MS}}$ and $\Omega_\chi h^2$. (In the last case the slightly skewed shape of the pdf’s is a result of our treatment of the theoretical uncertainty which is larger for larger $\Omega_\chi h^2$.) On the other hand, the electroweak observables m_W and $\sin^2 \theta_{\text{eff}}$ show some pull away from their expected values, in general agreement with ref. [15] where the two variables were computed with a similar precision. On the other hand, the tension is insufficient to provide convincing preference for low M_{SUSY} , in apparent contrast to the findings of ref. [36].

The biggest tension between best-fit values and experiment is displayed, unsurprisingly, in the SUSY contribution to the anomalous magnetic moment of the muon. For both signs of μ the peaks of the relative probability are far below the central experimental value (about 3.2σ for $\mu > 0$ versus about 3.7σ for $\mu < 0$), and close to each other [15]. We conclude that it is not justified to use this sole observable to select the positive sign of μ — one

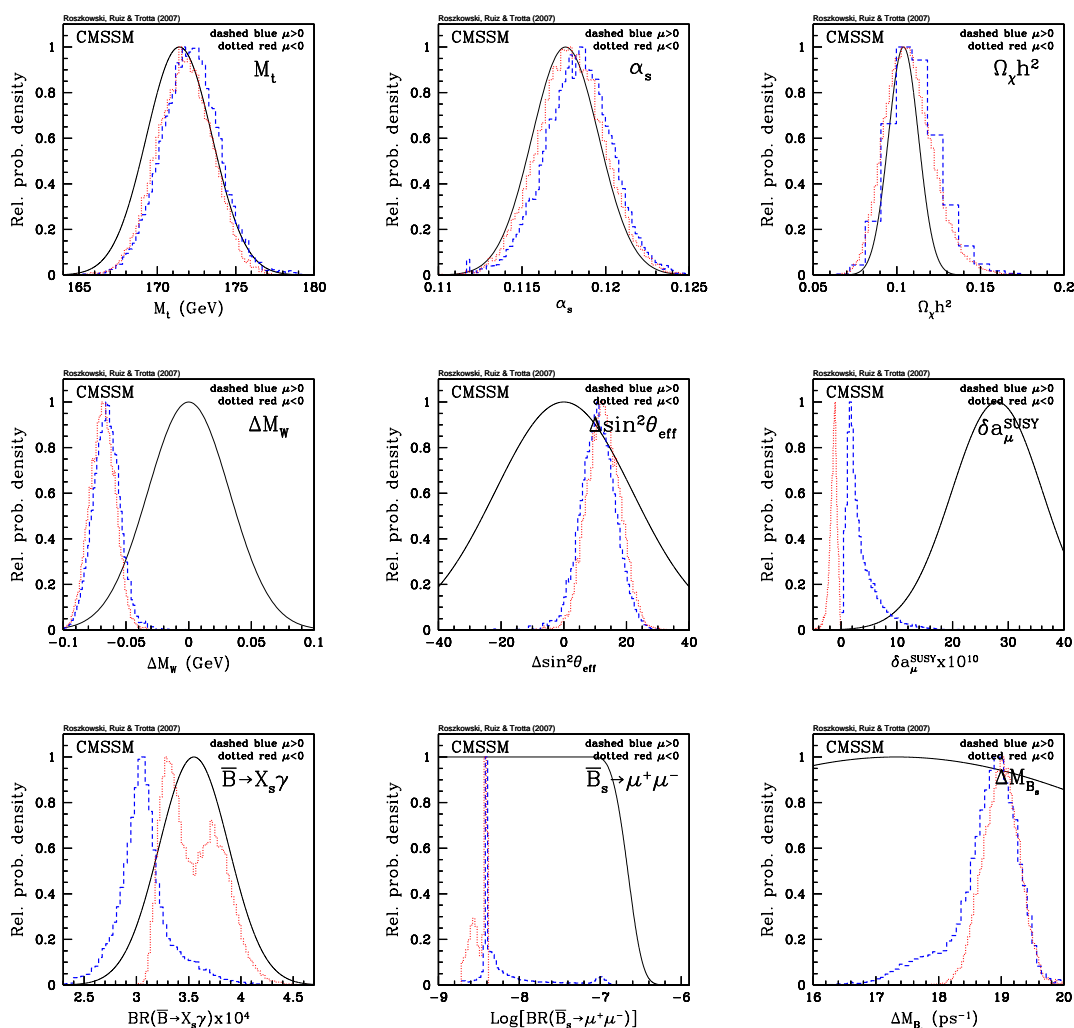


Figure 8: The 1-dim relative probability density functions for several variables: M_t , $\alpha_s(M_Z)^{\overline{MS}}$, $\Omega_\chi h^2$, $\Delta m_W = m_W - 80.392$ GeV, $\Delta \sin^2 \theta_{\text{eff}} = \sin^2 \theta_{\text{eff}} - 0.23153$, $BR(\overline{B} \rightarrow X_s \gamma)$, $\delta a_\mu^{\text{SUSY}}$, $BR(\overline{B}_s \rightarrow \mu^+ \mu^-)$, ΔM_{B_s} . In each panel the dashed blue (dotted red) curves correspond to $\mu > 0$ ($\mu < 0$) while the black solid line represents the data as encoded in the likelihood function. This figure should be compared with figure 10 in ref. [14].

has to perform a global fit in all of the variables and judge the two cases by this criterion. Furthermore, the new $BR(\overline{B} \rightarrow X_s \gamma)$ actually seems to agree with the data slightly better for $\mu < 0$ than for the other sign. Generally, for $\mu > 0$ the total $BR(\overline{B} \rightarrow X_s \gamma)$ remains peaked around the SM central value, while for $\mu < 0$ it is somewhat above it. Finally, $BR(\overline{B}_s \rightarrow \mu^+ \mu^-)$ and ΔM_{B_s} are peaked at their SM values, somewhat more so than before [14].

3.2 Implications for collider searches

In our Bayesian formalism, high probability ranges of the CMSSM parameters can easily

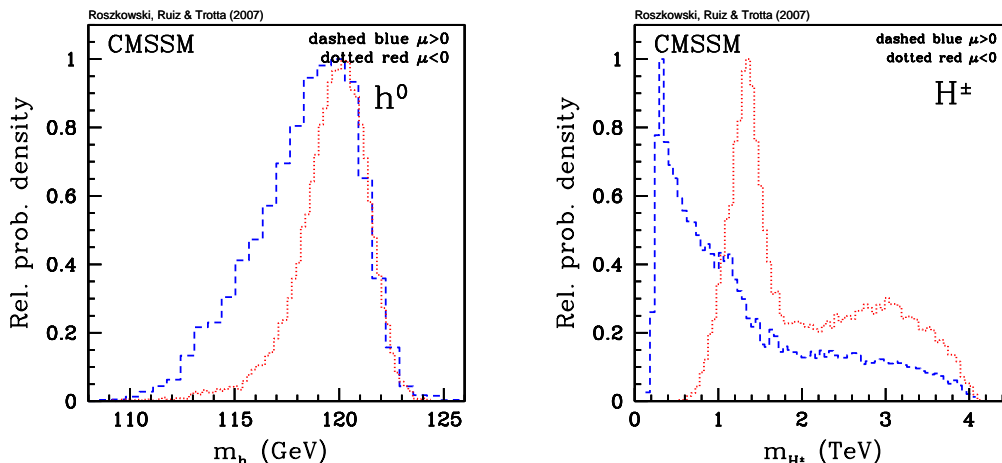


Figure 9: The 1-dim relative probability density functions for the masses of h^0 (left panel) and H^\pm (right panel). Dashed blue (dotted red) curves correspond to $\mu > 0$ ($\mu < 0$). Analogous and more detailed figures for the case $\mu > 0$ were presented in figure 7 of ref. [16].

be translated into analogous ranges for Higgs and superpartner masses, and for other observables, including indirect processes and dark matter detection cross sections. We discuss them in turn below.

We start with the Higgs bosons. In figure 9 we plot the Bayesian relative probability density distributions of the mass of the lightest Higgs boson h^0 and of the charged Higgs boson H^\pm for both signs of μ .⁸ (The other Higgs bosons are basically degenerate in mass with H^\pm .) In both cases we can see a clear peak in m_h close to 120 GeV, and a sharp drop-off for larger values of the mass. The other Higgs are typically considerably heavier for negative μ than for the other choice. This may provide one way of an experimental determination of the sign of μ . The 68% and 95% total probability ranges of the Higgs masses are given in table 4 below. We should also note that the alternative measure of the mean quality-of-fit favors lower ranges of the masses of all the Higgs bosons in the case of $\mu > 0$ [16]. For the case $\mu < 0$, the mean quality-of-fit distribution of m_h is roughly similar to that of the pdf but with the peak shifted to the right by about 1 GeV (plus some moderate preference for smaller values, around the current LEP-II limit), while the masses of all the other Higgs bosons are preferably very heavy, in the TeV regime.

In ref. [16] we have investigated in detail light Higgs masses and couplings for the case of $\mu > 0$. In particular we showed that, throughout the whole CMSSM parameter space, the couplings of the lightest Higgs boson h^0 to the gauge bosons Z and W are very close to those of the SM Higgs boson with the same mass, while its couplings to bottom quark and tau lepton pairs show some variation. We concluded that, at the Tevatron, with about 2fb^{-1} of integrated luminosity per experiment (already on tape), it should be possible to set a 95% CL exclusion limit for the whole 95% posterior probability range of m_h . Based

⁸The case of $\mu > 0$ was already presented in figure 7 of ref. [16]. We include it here for comparison.

Particle (TeV)	$\mu < 0$		$\mu > 0$	
	68%	95%	68%	95%
h^0	(0.1180, 0.1211)	(0.1151, 0.1223)	(0.1154, 0.1204)	(0.1125, 0.1219)
H^0, A^0, H^\pm	(1.2, 3.1)	(0.91, 3.8)	(0.36, 2.5)	(0.21, 3.6)
χ_1^0	(0.23, 0.67)	(0.11, 0.82)	(0.16, 0.49)	(0.06, 0.69)
χ_1^\pm	(0.3, 1.2)	(0.15, 1.4)	(0.25, 0.76)	(0.11, 1.2)
\tilde{g}	(1.4, 3.4)	(0.77, 4.0)	(1.0, 2.6)	(0.41, 3.5)
\tilde{e}_R	(1.8, 3.8)	(0.37, 4.0)	(1.5, 3.6)	(0.5, 4.0)
$\tilde{\nu}$	(1.9, 3.8)	(0.58, 4.0)	(1.6, 3.6)	(0.65, 4.0)
$\tilde{\tau}_1$	(1.4, 3.3)	(0.34, 3.8)	(0.80, 2.8)	(0.28, 3.7)
\tilde{q}_R	(2.9, 4.3)	(1.6, 4.9)	(1.9, 4.0)	(1.3, 4.7)
\tilde{t}_1	(1.9, 3.1)	(1.1, 3.6)	(1.3, 2.6)	(0.86, 3.3)
\tilde{b}_1	(2.3, 3.5)	(1.4, 4.1)	(1.4, 3.1)	(1.0, 3.8)

Table 4: Higgs boson and selected superpartner mass ranges (in TeV) containing 68% and 95% of posterior probability (with all other parameters marginalized over) for both signs of μ . Masses above 1 TeV have been rounded up to 1 significant digit.

on figure 9 and table 4 we extend this conclusion to the case of $\mu < 0$. On the optimistic side, should a Higgs signal be found, in order to be able to claim a 3σ evidence, at least about 4 fb^{-1} will be needed, independently of the sign of μ . The Tevatron’s ultimate goal is to collect about 8 fb^{-1} per experiment.

One should remember that the above conclusions do depend on the assumed prior range of $m_0 < 4 \text{ TeV}$, as well as on the choice of adopting flat priors in the CMSSM variables of eq. (2.1). For instance, adopting a much more generous upper limit $m_0 < 8 \text{ TeV}$ would lead to changing the ranges for $\mu > 0$ to roughly $120.4 \text{ GeV} \lesssim m_h \lesssim 124.4 \text{ GeV}$ (68% CL) and $115.4 \text{ GeV} \lesssim m_h \lesssim 125.6 \text{ GeV}$ (95% CL), the latter of which could be excluded at 95% CL with about 3 fb^{-1} of integrated luminosity per experiment [16]. Still, should no Higgs signal be found at the Tevatron, large ranges of m_0 will become excluded at high CL, with the specific value depending on the accumulated luminosity.

Turning next to superpartners, we show in figure 10 the relative pdf’s of the masses of several of them, while in table 4 we give the corresponding 68% and 95% probability ranges. The blue dashed curves are for $\mu > 0$ and the red dotted ones for $\mu < 0$. Firstly, for $\mu < 0$ all the scalar superpartners are considerably heavier than for the other sign of μ , as expected based on the discussion of most probable ranges of $m_{1/2}$ and especially m_0 . In fact, if $\mu < 0$ then all the sleptons and squarks (whose masses, except for the 3rd generation, are at least as large as m_0) may be beyond the reach of the LHC. For $\mu > 0$ there is a good chance of seeing the gluino (assuming the LHC reach of some $2.7 - 3 \text{ TeV}$) and a reasonable chance of seeing some squarks and sleptons. Unfortunately, these prospects are considerably less optimistic than what we found in figure 5 and table 6 of ref. [14], where the previous SM value of $BR(\bar{B} \rightarrow X_s \gamma)$ was used. A dedicated analysis would be required to derive more detailed conclusions.

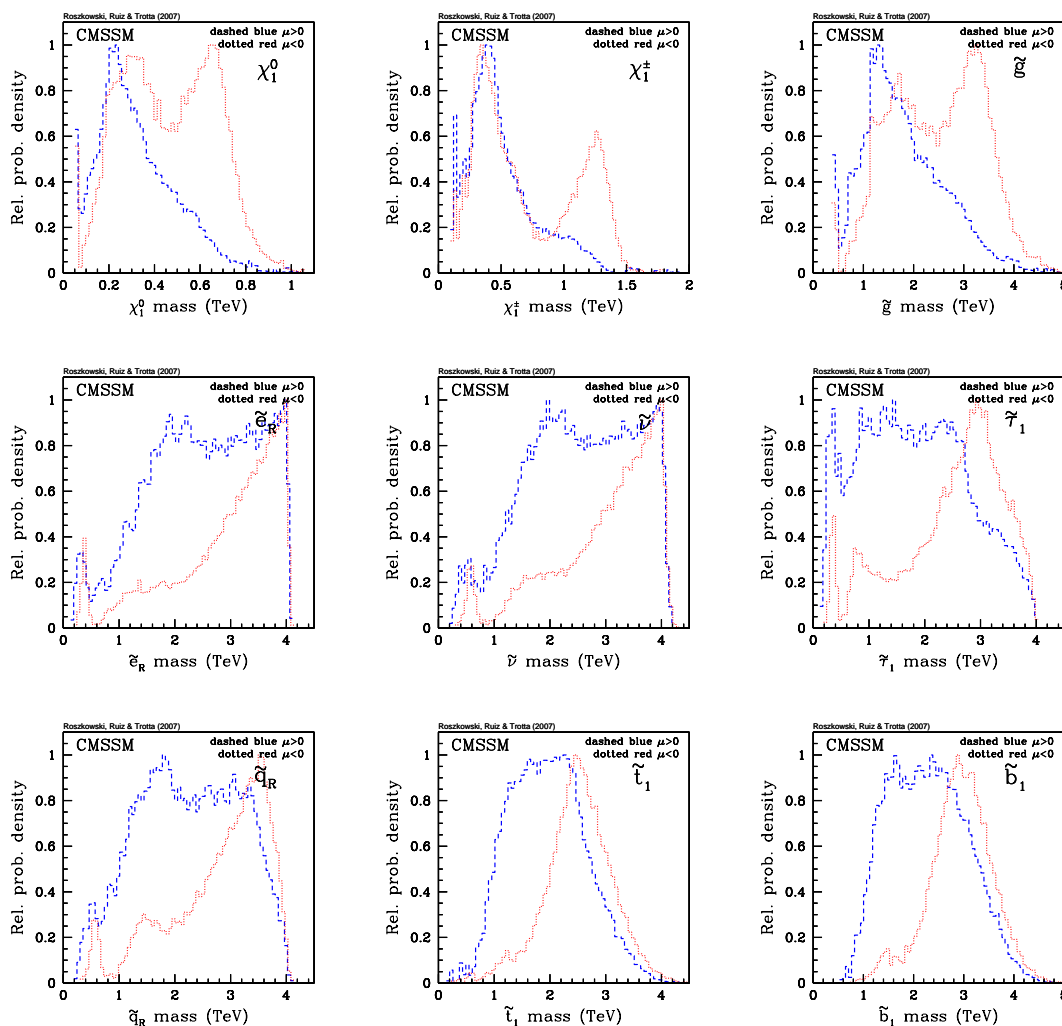


Figure 10: As in figure 3, but for the masses of several representative superpartners. This figure should be compared with figure 5 (black solid lines) in ref. [14].

3.3 Implications for direct detection of Dark Matter

We will now examine implications for direct detection of the lightest neutralino assumed to be the DM in the Universe, via its elastic scatterings with targets in underground detectors [4]. We will consider both spin-independent (SI) and spin-dependent (SD) interactions. The underlying formalism for both types of interactions can be found in several sources. (See, e.g., [4, 39–41].) In this analysis we use the expressions and inputs as presented in ref. [41]. We only note here that the SI interactions cross section σ_p^{SI} of a WIMP scattering off a proton in a target nucleus is the same as that of a neutron and that the total SI interactions cross section of the nucleus is proportional to σ_p^{SI} times the square of the mass number. In contrast, for the SD interactions, the cross section for a WIMP scattering off a proton, σ_p^{SD} , does not necessarily have to be the same as the one from a neutron [42, 43].

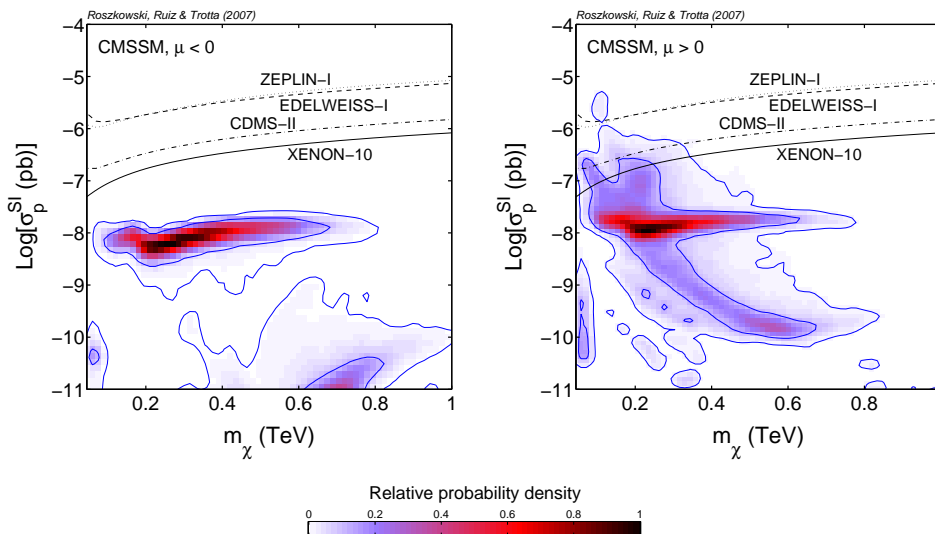


Figure 11: The 2-dim relative probability density for σ_p^{SI} vs. the neutralino mass m_χ for $\mu < 0$ (left panel) and $\mu > 0$ (right panel). The inner (outer) solid contours delimit the regions of 68% and 95% total probability, respectively. Some current experimental upper bounds are also shown. The right panel should be compared with figure 13 (top) in ref. [14].

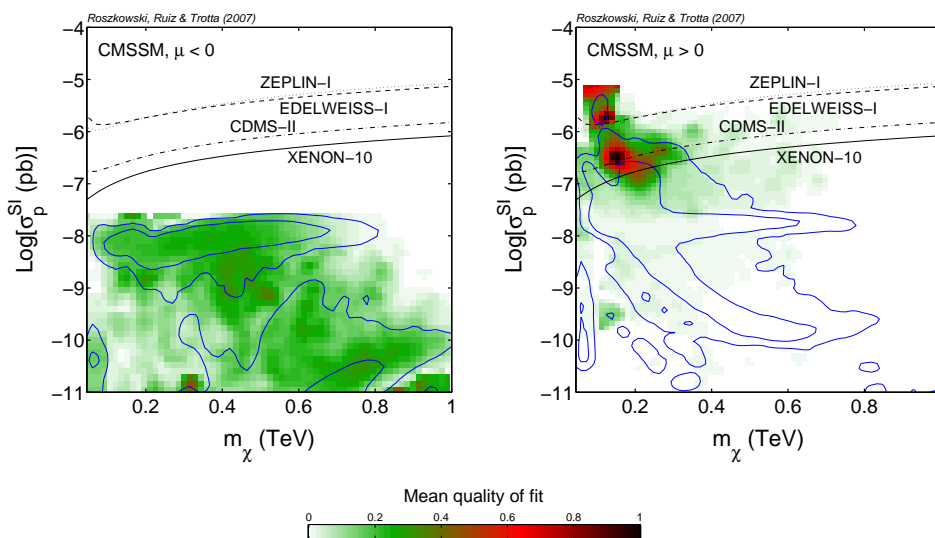


Figure 12: The mean quality-of-fit for σ_p^{SI} vs. the neutralino mass m_χ for $\mu < 0$ (left panel) and $\mu > 0$ (right panel). The inner (outer) solid contours delimit the regions of posterior 68% and 95% total probability, respectively (compare figure 11). Some current experimental upper bounds are also shown, but have not been included as constraints in the likelihood function. The right panel should be compared with figure 13 (bottom) in ref. [14].

In figure 11 we show the Bayesian posterior relative probability distribution in the usual plane of σ_p^{SI} and the DM neutralino mass m_χ for $\mu < 0$ (left panel) and $\mu > 0$ (right panel). Starting with $\mu > 0$, we can see a big concentration of probability density at rather

high values of $\sigma_p^{SI} \sim 10^{-8}$ pb, characteristic of the FP region of large m_0 [44], which is favored by the current theoretical evaluation of $BR(\overline{B} \rightarrow X_s \gamma)$, as we have seen above. In the FP region, the neutralino, while remaining predominantly bino-like, receives a sizable higgsino component, which strengthens the dominant Higgs-exchange contribution to σ_p^{SI} . In addition, there is a more well-known branch, with σ_p^{SI} decreasing with m_χ , which comes from the (now somewhat disfavored) region of $m_{1/2}, m_0 \lesssim 1$ TeV where the relic abundance $\Omega_\chi h^2$ of the neutralinos is reduced to agree with WMAP and other determinations by a pseudoscalar Higgs resonance in their pair annihilation and/or by their coannihilations with sleptons. In order to appreciate the change in the CMSSM predictions for σ_p^{SI} , the right panel should be compared with the top panel of figure 13 in ref. [14] where a previous value of the SM prediction for $BR(\overline{B} \rightarrow X_s \gamma)$ was used.

The left panel of figure 11 (the case of $\mu < 0$) also shows a strong preference for $\sigma_p^{SI} \sim 10^{-8}$ pb, which corresponds to the FP region at multi-TeV m_0 , as for the other sign of μ . In addition, we find another rather large 68% total probability region at extremely low value, below 10^{-10} pb, which corresponds to the higher probability region of $m_{1/2} \sim 1.5$ TeV in the $(m_{1/2}, m_0)$ plane. Such tiny values of σ_p^{SI} are a result of cancellation between the Higgs-exchange contribution to up- and down-type quarks [39, 40].

In both panels of figure 11 we have marked some of the current direct experimental upper limits [45–47], assuming a default value of 0.3 GeV/cm^3 for the local DM density. It is encouraging that experiments, notably XENON-10 with its very new limit, are already probing some portions of the CMSSM PS for $\mu > 0$. CDMS-II is currently taking data and is expecting to improve its limit to a similar level of sensitivity. Clearly, a further improvement by about an order of magnitude will constitute a critical leap as it will allow one to reach down to the heart of the SI interactions cross sections favored in the CMSSM. Future one-tonne detectors are expected to reach down to $\sigma_p^{SI} \gtrsim 10^{-10}$ pb, thus probing most of the favored parameter space of the CMSSM, at least for the more favored case of $\mu > 0$. We note that the probability of $\sigma_p^{SI} > 10^{-10}$ pb in figure 11 is 98.4% for $\mu > 0$ and 62.5% for $\mu < 0$.

It is worth re-emphasizing that, in addition to light Higgs searches at the Tevatron and the LHC, direct detection DM searches will provide an alternative experimental probe of the FP region at multi-TeV m_0 , in which the squarks will be too heavy to be produced at the LHC, although the gluino mass should remain mostly (partly) accessible for $\mu > 0$ ($\mu < 0$).

For comparison, figure 12 shows the ranges favored by the alternative measure of the mean quality-of-fit. Starting with the case of $\mu > 0$ (the right panel), we can see a handful of small regions of a rather large σ_p^{SI} , above a few times 10^{-7} pb, which are already in conflict with the current limit from the XENON-10. These cases corresponds to the “islands” of good fit to the data that we have already seen in figure 6, where they are all concentrated in the region of $m_{1/2} \lesssim 0.5$ TeV and $m_0 \lesssim 1.5$ TeV. With a modest improvement of sensitivity, DM search experiments will be able to probe the entire region favored by the mean quality-of-fit in the case of $\mu > 0$. (Notice that neither the posterior pdf nor the mean quality-of-fit give much preference for very small σ_p^{SI} .) In contrast, for $\mu < 0$ (the

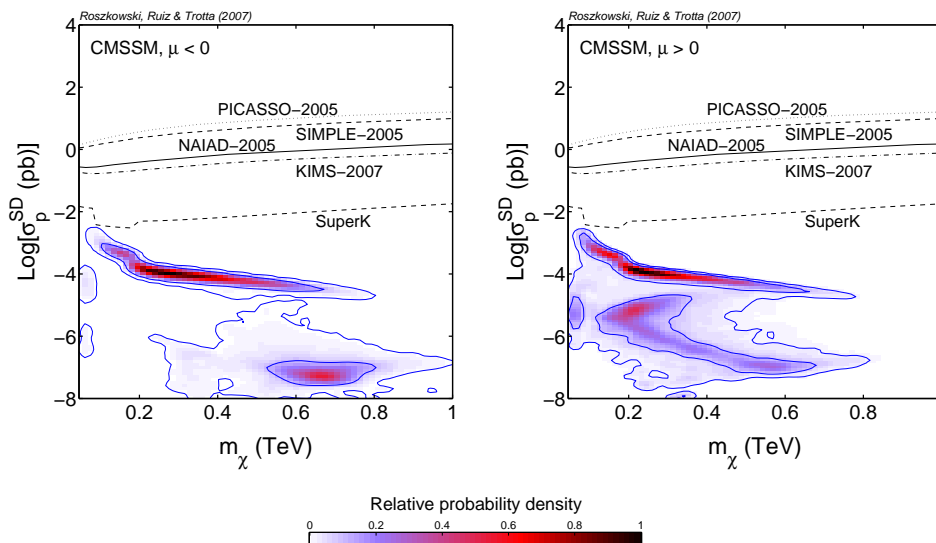


Figure 13: The 2-dim relative probability density of σ_p^{SD} vs. the neutralino mass m_χ for $\mu < 0$ (left panel) and $\mu > 0$ (right panel). The inner (outer) solid contours delimit the regions of 68% and 95% total probability, respectively. Some current experimental 90% CL upper bounds are also shown. Analogous plots for σ_n^{SD} are basically identical but the experimental limits from direct detection are weaker by nearly two orders of magnitude.

left panel of figure 12) there is hardly any region giving good quality fits for $\sigma_p^{SI} > 10^{-11}$ pb. This is a reflection of what we have already seen in the $(m_{1/2}, m_0)$ plane in figure 7.

Turning next to SD interactions, in figure 13 we present the relative probability density for neutralino-proton scattering cross section σ_p^{SD} versus m_χ for $\mu < 0$ (left panel) and $\mu > 0$ (right panel). In the FP region the increased higgsino component of the neutralino in this case leads to a larger coupling to the dominant Z -boson exchange. This is reflected in the figure where the highest probability regions are, for both signs of μ , concentrated around $\sigma_p^{SD} \sim 10^{-4}$ pb. For $\mu > 0$ there is an additional higher probability region which is visible in the right panel, and which corresponds to the Higgs resonance and coannihilation region mentioned above. In the case of $\mu < 0$ instead, an additional higher probability region is visible in the left panel at $\sigma_p^{SD} \lesssim 10^{-7}$ pb and $m_\chi \sim 0.7$ TeV. It corresponds to the region of $m_{1/2} \sim 1.5$ TeV in the $(m_{1/2}, m_0)$ plane (figure 2).

The current experimental upper limits [48–51] from direct searches, assuming a default value of $0.3 \text{ GeV}/\text{cm}^3$ for the local DM density, as well as an indirect limit from neutralino annihilations into neutrinos in the Sun, the Earth or the Galactic center [52], which have also been shown in figure 13, still remain a few order of magnitude above the predictions of the CMSSM. On the other hand, experimental sensitivity has undergone steady progress also in the case of SD interactions. Eventually, it will be important to reach down below the level of $\sigma_p^{SD} \lesssim 10^{-4}$ pb, which would allow one for an independent cross-check of CMSSM predictions for dark matter.

In table 5 we have listed the ranges of both σ_p^{SI} and σ_p^{SD} containing 68% and 95% of posterior probability (with all other parameters marginalized over) for both signs of μ .

	Spin-independent cross section σ_p^{SI} (pb)	
	68%	95%
$\mu < 0$	$(2.9 \times 10^{-12}, 8.1 \times 10^{-9})$	$(1.6 \times 10^{-13}, 1.4 \times 10^{-8})$
$\mu > 0$	$(2.8 \times 10^{-10}, 3.9 \times 10^{-8})$	$(7.2 \times 10^{-11}, 2.5 \times 10^{-7})$
	Spin-dependent cross section σ_p^{SD} (pb)	
	68%	95%
$\mu < 0$	$(5.3 \times 10^{-8}, 9.6 \times 10^{-5})$	$(1.7 \times 10^{-8}, 4.4 \times 10^{-4})$
$\mu > 0$	$(2.0 \times 10^{-7}, 8.9 \times 10^{-5})$	$(4.2 \times 10^{-8}, 4.9 \times 10^{-4})$

Table 5: Direct detection of dark matter: ranges of spin-independent and spin-dependent cross section encompassing 68% and 95% of posterior probability (with all other parameters marginalized over) for both signs of μ .

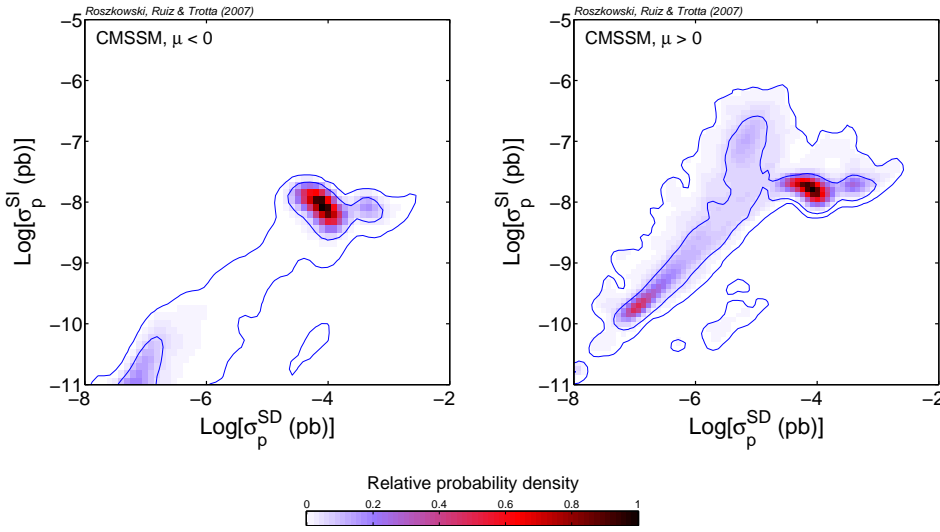


Figure 14: The 2-dim relative probability density of σ_p^{SI} vs. σ_p^{SD} for $\mu < 0$ (left panel) and $\mu > 0$ (right panel). The inner (outer) solid contours delimit the regions of 68% and 95% total probability, respectively. All other parameters have been marginalized over.

The ranges cover the whole allowed range of m_χ and provide supplementary information to what one can read off from figures 11 and 13.

As mentioned above, in the SD interaction case the cross section of WIMP scattering from a neutron can in general be very different from the one from a proton. However, in our scan of the CMSSM, we have found its relatively probability distribution versus m_χ to be very close to the case with the proton, and thus do not show it here. As regards the mean quality-of-fit (not shown for σ_p^{SD}), at $\mu > 0$ the best-fit regions in figure 6 give a rather small value of $\sim 10^{-5}$ pb.

3.4 Correlations among observables

The Bayesian approach employed in this analysis makes it very easy to examine various possible global correlations among different observables in the CMSSM. For example, in

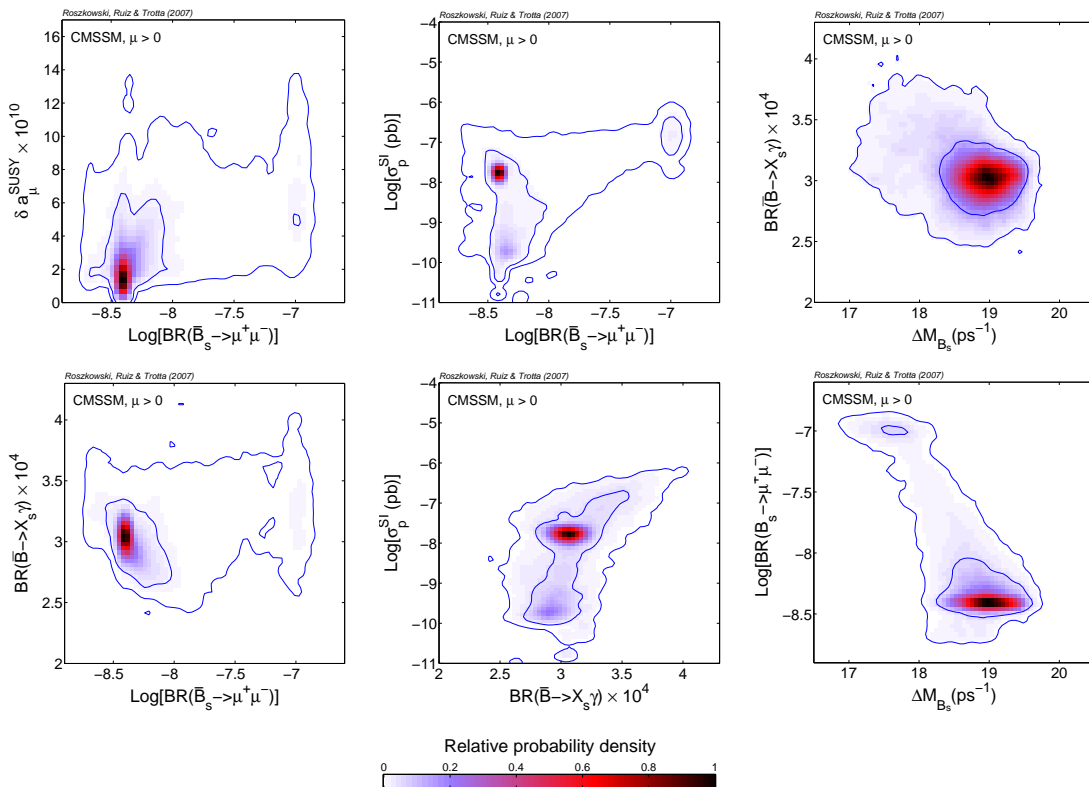


Figure 15: The 2-dim relative probability density for pairs of selected variables for $\mu > 0$. The inner (outer) solid contours delimit the regions of 68% and 95% total probability, respectively. All other parameters have been marginalized over. This figure should be compared with figure 14 in ref. [14].

figure 14 we present the 2-dim pdf of σ_p^{SI} versus σ_p^{SD} for $\mu < 0$ (left panel) and $\mu > 0$ (right panel). For both signs of μ we can see a big concentration of probability density on $\sigma_p^{SI} \sim 10^{-8}$ pb and $\sigma_p^{SD} \sim 10^{-4}$ pb, which is a reflection of their behavior in figure 11 and figure 13, respectively — an effect of the FP region. For $\mu > 0$ we can see an additional feature of a positive correlation which is due to the contribution from the Higgs resonance and/or coannihilation effects.

More correlations are displayed in figure 15 for the case of $\mu > 0$. Again, the effect of the FP region is overwhelming. In all the observables, other than the dark matter SI cross section, SUSY effects are likely to be tiny — the probability density is clearly peaked at the respective SM values. For $\mu < 0$ (not displayed) the concentration is typically even stronger. Figure 15 should be compared with figure 14 of ref. [14] in order to appreciate the change. Some correlations which were quite well pronounced in that figure (eg. in σ_p^{SI} versus $BR(\bar{B}_s \rightarrow \mu^+ \mu^-)$) are now barely visible.

4. Summary and conclusions

We have applied the highly efficient MCMC scanning method to explore the parameter

space of the CMSSM and outlined the regions favored by the Bayesian posterior probability and, for comparison, by the mean quality-of-fit. We assumed flat priors in the usual CMSSM parameters, applied and updated all relevant experimental constraints from colliders and cosmological dark matter abundance, while paying particular attention to the impact of the recent change in the SM value of $BR(\bar{B} \rightarrow X_s \gamma)$. We examined both signs of μ . For both choices, we found strong preference for the focus point region with large m_0 in the few TeV range (for $\mu < 0$ actually saturating at the assumed prior boundary of 4 TeV), and not as large $m_{1/2} \lesssim 2$ TeV. For comparison, the mean quality-of-fit measure selected a small number of isolated regions giving good fit to the data for $\mu > 0$. It appears that the choice $\mu < 0$ is more at odds with the data, as reflected by its worse quality-of-fit.

We then examined ensuing implications for Higgs and superpartner searches and for direct detection of dark matter. Prospects for the Tevatron of excluding the whole 95% CL range of m_h remain very good, or else there is very good hope to see at least some evidence of a signal with the expected final integrated luminosity. Scalar superpartner masses are typically heavier than 1 TeV (compare table 4) but there is a reasonable chance for at least some squarks (but probably no sleptons) to be seen at the LHC. On the other hand, the gluino, while also preferably heavy, should have a much better chance of discovery at the LHC. Prospects for detection are also promising in direct detection searches for dark matter which are sensitive to spin-independent interactions. An improvement in sensitivity down to $\sigma_p^{SI} \sim 10^{-8}$ pb will allow CDMS-II and other experiments to reach down to the bulk of the values favored by the posterior pdf (for both signs of μ), and actually to fully explore all best-fit regions in the preferred case of $\mu > 0$. On the other hand, an improvement in sensitivity of at least 3 orders of magnitude will be required before favored ranges of cross sections for spin-dependent neutralino-proton interactions are tested by experiment.

We stress that some of our findings do depend on our choice of the (usual) variables m_0 , $m_{1/2}$, A_0 and, especially, $\tan \beta$ as CMSSM parameters over which we take flat priors. Of particular relevance is the upper bound $m_0 < 4$ TeV. Other choices are possible and should be examined. (See refs. [13, 53] and Note Added below.) The choice of CMSSM parameters and flat priors that we have made in the present analysis and the comparison with the mean-quality-of-fit statistics are meant to facilitate comparison with fixed-grid studies using similar assumptions.

Note added. Very recently, after our analysis was completed, a new paper of Allanach et al., [53] has appeared. The authors argue that, instead of assuming a flat prior in $\tan \beta$, it is more natural to use a “REWSB prior” where μ and the bi-linear soft mass parameter B are taken as inputs with flat distributions. Whether this choice (originally advocated by R. Ratazzi) is superior to any other is debatable but it is certainly justifiable to apply it, at least for the sake of examining the sensitivity of observables to the choice of priors. We note that with the REWSB prior the preference for large m_0 , well above 1 TeV, still remains. (A more detailed comparison is difficult because in ref. [53] a previous SM value of $BR(\bar{B} \rightarrow X_s \gamma)$ has been used.) On the other hand, the authors in addition choose to give strong preference to cases where all the CMSSM mass parameters are of the same order. In our opinion this assumption does reflect a certain level of theoretical bias which at the

end strongly changes the conclusions obtained with the REWSB prior only. (In particular it disfavors the focus point region which, as we have shown, can be seen as being favored by the current results on $BR(\bar{B} \rightarrow X_s \gamma)$.) We would prefer to see the lack of the hierarchy of the CMSSM mass parameters to be an outcome of applying experimental constraints, rather than of applying theoretical prejudice.

Acknowledgments

We are indebted to M. Misiak for providing to us a part of his code computing the SM value of $BR(\bar{B} \rightarrow X_s \gamma)$ and for several clarifying comments about the details of the calculation. L.R is partially supported by the EC 6th Framework Programmes MRTN-CT-2004-503369 and MRTN-CT-2006-035505. R.RdA is supported by the program “Juan de la Cierva” of the Ministerio de Educación y Ciencia of Spain. RT is supported by the Lockyer Fellowship of the Royal Astronomical Society and by St Anne’s College, Oxford. The author(s) would like to thank the European Network of Theoretical Astroparticle Physics ENTApP ILLIAS/N6 under contract number RII3-CT-2004-506222 for financial support. This project benefited from the CERN-ENTApP joint visitor’s programme on dark matter, 5-9 March 2007.

References

- [1] H.E. Haber and G.L. Kane, *The search for supersymmetry: probing physics beyond the standard model*, *Phys. Rept.* **117** (1985) 75;
S.P. Martin, *A supersymmetry primer*, hep-ph/9709356.
- [2] G.L. Kane, C.F. Kolda, L. Roszkowski and J.D. Wells, *Study of constrained minimal supersymmetry*, *Phys. Rev. D* **49** (1994) 6173 [hep-ph/9312272].
- [3] H.P. Nilles, *Supersymmetry, supergravity and particle physics*, *Phys. Rept.* **110** (1984) 1;
A. Brignole, L.E. Ibáñez and C. Muñoz, *Soft supersymmetry-breaking terms from supergravity and superstring models*, hep-ph/9707209.
- [4] See, e.g., G. Jungman, M. Kamionkowski and K. Griest, *Supersymmetric dark matter*, *Phys. Rept.* **267** (1996) 195 [hep-ph/9506380];
C. Muñoz, *Dark matter detection in the light of recent experimental results*, *Int. J. Mod. Phys. A* **19** (2004) 3093 [hep-ph/0309346].
- [5] HEAVY FLAVOR AVERAGING GROUP (HFAG) collaboration, E. Barberio et al., *Averages of b-hadron properties at the end of 2005*, hep-ex/0603003; for a very recent update see *Averages of b-hadron properties at the end of 2006*, arXiv:0704.3575.
- [6] M. Misiak and M. Steinhauser, *Nnlo QCD corrections to the $\bar{B} \rightarrow X_s \gamma$ matrix elements using interpolation in m_c* , *Nucl. Phys. B* **764** (2007) 62 [hep-ph/0609241].
- [7] M. Misiak et al., *The first estimate of $\bar{B} \rightarrow X_s \gamma$ at $\mathcal{O}(\alpha_s^2)$* , *Phys. Rev. Lett.* **98** (2007) 022002 [hep-ph/0609232].
- [8] T. Becher and M. Neubert, *Analysis of $Br(B \rightarrow X_s \gamma)$ at NNLO with a cut on photon energy*, *Phys. Rev. Lett.* **98** (2007) 022003 [hep-ph/0610067].

- [9] PARTICLE DATA GROUP, W.-M. Yao et al., *Review of particle physics*, *J. Phys. G* **33** (2006) 1.
- [10] See, e.g., B.A. Berg, *Markov chain Monte Carlo simulations and their statistical analysis*, World Scientific, Singapore (2004).
- [11] E.A. Baltz and P. Gondolo, *Markov chain Monte Carlo exploration of minimal supergravity with implications for dark matter*, *JHEP* **10** (2004) 052 [[hep-ph/0407039](#)].
- [12] B.C. Allanach and C.G. Lester, *Multi-dimensional MSUGRA likelihood maps*, *Phys. Rev. D* **73** (2006) 015013 [[hep-ph/0507283](#)].
- [13] B.C. Allanach, *Naturalness priors and fits to the constrained minimal supersymmetric standard model*, *Phys. Lett. B* **635** (2006) 123 [[hep-ph/0601089](#)].
- [14] R.R. de Austri, R. Trotta and L. Roszkowski, *A Markov chain Monte Carlo analysis of the CMSSM*, *JHEP* **05** (2006) 002 [[hep-ph/0602028](#)];
see also R. Trotta, R.R. de Austri and L. Roszkowski, *Prospects for direct dark matter detection in the constrained MSSM*, *New Astron. Rev.* **51** (2007) 316 [[astro-ph/0609126](#)].
- [15] B.C. Allanach, C.G. Lester and A.M. Weber, *The dark side of msugra*, *JHEP* **12** (2006) 065 [[hep-ph/0609295](#)].
- [16] L. Roszkowski, R.R. de Austri and R. Trotta, *On the detectability of the cmssm light Higgs boson at the Tevatron*, *JHEP* **04** (2007) 084 [[hep-ph/0611173](#)].
- [17] R. Trotta, R.R. de Austri and L. Roszkowski, *Prospects for direct dark matter detection in the constrained MSSM*, *New Astron. Rev.* **51** (2007) 316 [[astro-ph/0609126](#)].
- [18] J.L. Feng, K.T. Matchev and T. Moroi, *Multi-TeV scalars are natural in minimal supergravity*, *Phys. Rev. Lett.* **84** (2000) 2322 [[hep-ph/9908309](#)]; *Focus points and naturalness in supersymmetry*, *Phys. Rev. D* **61** (2000) 075005 [[hep-ph/9909334](#)].
- [19] TEVATRON ELECTROWEAK WORKING GROUP collaboration, E. Brubaker et al., *Combination of CDF and D0 results on the mass of the top quark*, [hep-ex/0608032](#).
- [20] CDF collaboration, *A combination of CDF and D0 results on the mass of the top quark*, [hep-ex/0703034](#).
- [21] See <http://lepewwg.web.cern.ch/LEPEWWG>.
- [22] CDF - RUN II collaboration, A. Abulencia et al., *Measurement of the $B_s - \bar{B}_s$ oscillation frequency*, *Phys. Rev. Lett.* **97** (2006) 062003 [[hep-ex/0606027](#)];
CDF collaboration, A. Abulencia et al., *Observation of $B_s - \bar{B}_s$ oscillations*, *Phys. Rev. Lett.* **97** (2006) 242003 [[hep-ex/0609040](#)].
- [23] WMAP collaboration, D.N. Spergel et al., *Wilkinson Microwave Anisotropy Probe (WMAP) three year results: implications for cosmology*, [astro-ph/0603449](#).
- [24] CDF collaboration, *Search for $B_s \rightarrow \mu^+ \mu^-$ and $B_d \rightarrow \mu^+ \mu^-$ decays in $p\bar{p}$ collisions with CDF-II*, CDF note 8176 (June 2006).
- [25] The LEP Higgs Working Group, <http://lephiggs.web.cern.ch/LEPHIGGS>;
LEP WORKING GROUP FOR HIGGS BOSON SEARCHES collaboration, R. Barate et al., *Search for the standard model Higgs boson at LEP*, *Phys. Lett. B* **565** (2003) 61 [[hep-ex/0306033](#)].

- [26] M. Awramik, M. Czakon, A. Freitas and G. Weiglein, *Precise prediction for the W-boson mass in the standard model*, *Phys. Rev. D* **69** (2004) 053006 [[hep-ph/0311148](#)]; *Complete two-loop electroweak fermionic corrections to $\sin^2 \theta_{\text{eff}}$ and indirect determination of the Higgs boson mass*, *Phys. Rev. Lett.* **93** (2004) 201805 [[hep-ph/0407317](#)].
- [27] A. Djouadi et al., *Leading QCD corrections to scalar quark contributions to electroweak precision observables*, *Phys. Rev. D* **57** (1998) 4179 [[hep-ph/9710438](#)].
- [28] K. Hagiwara, A.D. Martin, D. Nomura and T. Teubner, *Improved predictions for $g-2$ of the muon and $\alpha_{\text{qed}}(m_z^2)$* , *Phys. Lett. B* **649** (2007) 173 [[hep-ph/0611102](#)].
- [29] G. Degrossi, P. Gambino and G.F. Giudice, *$B \rightarrow X_s \gamma$ in supersymmetry: large contributions beyond the leading order*, *JHEP* **12** (2000) 009 [[hep-ph/0009337](#)].
- [30] P. Gambino and M. Misiak, *Quark mass effects in $\bar{B} \rightarrow X_s \gamma$* , *Nucl. Phys. B* **611** (2001) 338 [[hep-ph/0104034](#)].
- [31] K.-i. Okumura and L. Roszkowski, *Weakened constraints from $b \rightarrow s \gamma$ on supersymmetry flavor mixing due to next-to-leading-order corrections*, *Phys. Rev. Lett.* **92** (2004) 161801 [[hep-ph/0208101](#)]; *Large beyond-leading-order effects in $b \rightarrow s \gamma$ in supersymmetry with general flavor mixing*, *JHEP* **10** (2003) 024 [[hep-ph/0308102](#)].
- [32] J. Foster, K.-i. Okumura and L. Roszkowski, *New Higgs effects in B-physics in supersymmetry with general flavour mixing*, *Phys. Lett. B* **609** (2005) 102 [[hep-ph/0410323](#)]; *Probing the flavour structure of supersymmetry breaking with rare B-processes: a beyond leading order analysis*, *JHEP* **08** (2005) 094 [[hep-ph/0506146](#)].
- [33] P. Gondolo et al., *DARKSUSY: computing supersymmetric dark matter properties numerically*, *JCAP* **07** (2004) 008 [[astro-ph/0406204](#)]; <http://www.physto.se/edsjo/darksusy/>.
- [34] J. Foster, K.-i. Okumura and L. Roszkowski, *Current and future limits on general flavour violation in $b \rightarrow s$ transitions in minimal supersymmetry*, *JHEP* **03** (2006) 044 [[hep-ph/0510422](#)]; *New constraints on SUSY flavour mixing in light of recent measurements at the Tevatron*, *Phys. Lett. B* **641** (2006) 452 [[hep-ph/0604121](#)].
- [35] B.C. Allanach, *SOFTSUSY: a C++ program for calculating supersymmetric spectra*, *Comput. Phys. Commun.* **143** (2002) 305 [[hep-ph/0104145](#)].
- [36] J.R. Ellis, S. Heinemeyer, K.A. Olive and G. Weiglein, *Indirect sensitivities to the scale of supersymmetry*, *JHEP* **02** (2005) 013 [[hep-ph/0411216](#)]; *Phenomenological indications of the scale of supersymmetry*, *JHEP* **05** (2006) 005 [[hep-ph/0602220](#)].
- [37] R. Trotta, *Applications of bayesian model selection to cosmological parameters*, *Mon. Not. Roy. Astron. Soc.* **378** (2007) 72 [[astro-ph/0504022](#)].
- [38] C. Gordon and R. Trotta, *Bayesian calibrated significance levels applied to the spectral tilt and hemispherical asymmetry*, [arXiv:0706.3014](#).
- [39] M. Drees and M. Nojiri, *Neutralino - nucleon scattering revisited*, *Phys. Rev. D* **48** (1993) 3483 [[hep-ph/9307208](#)].
- [40] J.R. Ellis, A. Ferstl and K.A. Olive, *Re-evaluation of the elastic scattering of supersymmetric dark matter*, *Phys. Lett. B* **481** (2000) 304 [[hep-ph/0001005](#)].

- [41] Y.G. Kim, T. Nihei, L. Roszkowski and R. Ruiz de Austri, *Upper and lower limits on neutralino wimp mass and spin-independent scattering cross section and impact of new $(g-2)_\mu$ measurement*, *JHEP* **12** (2002) 034 [[hep-ph/0208069](#)].
- [42] J.D. Lewin and P.F. Smith, *Review of mathematics, numerical factors, and corrections for dark matter experiments based on elastic nuclear recoil*, *Astropart. Phys.* **6** (1996) 87.
- [43] D.R. Tovey, R.J. Gaitskell, P. Gondolo, Y. Ramachers and L. Roszkowski, *A new model-independent method for extracting spin-dependent cross section limits from dark matter searches*, *Phys. Lett.* **B 488** (2000) 17 [[hep-ph/0005041](#)].
- [44] J.L. Feng, K.T. Matchev and F. Wilczek, *Neutralino dark matter in focus point supersymmetry*, *Phys. Lett.* **B 482** (2000) 388 [[hep-ph/0004043](#)].
- [45] CDMS collaboration, D.S. Akerib et al., *Limits on spin-independent WIMP-nucleon interactions from the two-tower run of the cryogenic dark matter search*, *Phys. Rev. Lett.* **96** (2006) 011302 [[astro-ph/0509259](#)].
- [46] THE EDELWEISS collaboration, V. Sanglard et al., *Final results of the EDELWEISS-I dark matter search with cryogenic heat-and-ionization Ge detectors*, *Phys. Rev.* **D 71** (2005) 122002 [[astro-ph/0503265](#)].
- [47] UK DARK MATTER collaboration, G.J. Alner et al., *First limits on nuclear recoil events from the ZEPLIN-I galactic dark matter detector*, *Astropart. Phys.* **23** (2005) 444.
- [48] PICASSO collaboration, M. Barnabe-Heider et al., *Improved spin dependent limits from the picasso dark matter search experiment*, *Phys. Lett.* **B 624** (2005) 186 [[hep-ex/0502028](#)].
- [49] T.A. Girard et al., *Simple dark matter search results*, *Phys. Lett.* **B 621** (2005) 233 [[hep-ex/0505053](#)].
- [50] UK DARK MATTER collaboration, G.J. Alner et al., *Limits on WIMP cross-sections from the NAIAD experiment at the boulby underground laboratory*, *Phys. Lett.* **B 616** (2005) 17 [[hep-ex/0504031](#)].
- [51] KIMS collaboration, H.S Lee et al., *Limits on WIMP-nucleon cross section with CsI(Tl) crystal detectors*, [arXiv:0704.0423](#).
- [52] SUPER-KAMIOKANDE collaboration, S. Desai et al., *Search for dark matter WIMPS using upward through-going muons in Super-Kamiokande*, *Phys. Rev.* **D 70** (2004) 083523 [*Erratum ibid.* **D 70** (2004) 109901] [[hep-ex/0404025](#)].
- [53] B.C. Allanach, C.G. Lester and A.M. Weber, *Natural priors, CMSSM fits and LHC weather forecasts*, [arXiv:0705.0487](#).

Erratum

The correct address of the Instituto de Física Teórica is:

*Instituto de Física Teórica UAM-CSIC, Facultad de Ciencias C-XVI,
Universidad Autónoma de Madrid, Cantoblanco, Madrid 28049, Spain*

JHEP07(2007)075